VIRTUAL FLUOROSCOPY SYSTEM FOR ARTHROSCOPIC SURGICAL TRAINING

VIRTUAL FLUOROSCOPY SYSTEM FOR ARTHROSCOPIC SURGICAL TRAINING

By

ZAHRA HOSSEINI

B.ENG.

A Thesis

Submitted to the School of Graduate Studies in Partial Fulfilment of the

Requirements for the Degree of Master of Applied Science

Master of Applied Science (2013)

School of Biomedical Engineering

McMaster University, Hamilton, Ontario, Canada

TITLE:	VIRTUAL FLUOROSCOPY SYSTEM FOR ARTHROSCOPIC SURGICAL TRAINING
AUTHOR:	Zahra Hosseini B.Eng., Electrical Engineering McMaster University, Hamilton, Ontario, 2011
SUPERVISORS:	Dr. Gregory Wohl, Dr. Shahram Shirani
NUMBER OF PAGES:	xvi, 105

Abstract

Minimally invasive operations have gained popularity over open surgical procedures in the recent years. These procedures, require the surgeon to perform highly specialized tasks including manipulation of tools through small incisions on the surface of the skin while looking at the images that are displayed on a screen. Therefore, effective training is required for the surgeons prior to performing such procedures on patients.

In this thesis I explored a novel idea for creating a training system for arthroscopic surgery. Previously obtained CT images of a patient model and the surgical tools are manipulated to create a library of fluoroscopy images. The surgical tools are tracked (a mechanical tracker and an electromagnetic tracker used in each iterations) in order to generate a spacial relationship between the patient model and the surgical tools. The position and orientation information from the tracking system is translated into the image coordinate frame. These homologous points in the two images (of surgical tools and the patient model), are used to co-register and overlay the two images and create a virtual fluoroscopy image.

The output image and the system performance was found to be very good and quite similar to that of a fluoroscopy system. The registration accuracy was evaluated using Root Mean Square Target Registration Error (RMS TRE). The RMS TRE for the system setup with the mechanical tracker was evaluated at 2.0 mm, 2.1 mm, and 2.5 mm, for 4, 5, and 6 control points, respectively. In the system setup with the electromagnetic tracking system the RMS TRE was evaluated at 7.6 mm, 12.4 mm,

and 11.3 mm, for 5, 7, and 9 control points, respectively. The acceptable range of error for arthroscopy procedures has been proposed to be 1-2 mm.

It was concluded that by using a tracking system, which is not prone to interference and allows for a wide range of motion this system can be completed to the point of manufacturing and use in training new surgeons.

To my parents and to my sisters, the support and love of whom I could not finish this work without.

Acknowledgments

I would like to thank my supervisor Dr. Gregory Wohl who always welcomed my opinion and encouraged me. I also want to thank Dr. Shahram Shirani, my co-supervisor, for all his help and support in the process of design and development of this project. Completion of this work would have been very difficult and cumbersome without their invaluable comments and suggestions. I also want to thank Dr. Ivan Wong who kindly created the opportunity for me to attend several operations in Halifax. This experience made it quite easy for me to define a framework for this project.

Besides my supervisors, a number of faculty members at the Electrical Engineering Department made the process of learning and conducting research much easier for me. I want to thank Dr. Shahin Sirouspour for all his guidance and help, as well as the resources he provided for me, during the development of this project. I want to thank Dr. Alexander Patriciu for his opinions and guidance. I also would like to thank Dr. Mike Noseworthy and Dr. Tom Chow for their time and tremendous help with the medical imaging portion of this work. I want to, also, thank DePuy Synthes Mitek Sports Medicine Inc. for providing me with the hip joint model.

Special friends and my family made the past two years very easy on me. I want to thank Matthaios for being such a great friend. I also want to thank Ashraf Atalla and Bahram Marami for their valuable opinions and for sharing their experience of graduate work with me. I want to thank my sisters, Boshra and Shera, for being there every step of the way during the past two years and throughout my life. I

want to send special thanks and appreciation to my parents who always believed in me and supported me in any way possible. Last but surely not the least, I want to thank Natalie Illingworth for all her useful and helpful followups on the numerous paperwork that must have been done prior to my graduation.

Contents

List of Figures

List of Tables

List of Abbreviations

AC	:	Alternate Current
DC	:	Direct Current
2D	:	2 Dimensional
3D	:	3 Dimensional
AP	:	Antero-Posterior
RF	:	Radio-Frequency
CT	:	Computed Tomography
VR	:	Virtual Reality
ACL	:	Antero Cruciate Ligament
PCL	:	Posterior Cruciate Ligament
MTS	:	Mechanical Tracking System
OTS	:	Optical Tracking System
UTS	:	Ultrasonic Tracking System
EMTS	:	Electromagnetic Tracking System
HMD	:	Head-Mounted Display

Declaration of Academic Achievement

I, Zahra Hosseini, performed all the work, including software development and testing, presented in this thesis and am responsible for the content. My supervisors, Dr. Gregory Wohl and Dr. Shahram Shirani, provided me with guidance in completing this work..

CHAPTER 1

Introduction

Arthroscopic surgery is a minimally invasive procedure that allows for repair of injuries or correction of anatomical abnormalities through very small incisions close to the joint. In comparison to open surgery, which is the traditional approach in performing surgical procedures on the joints, arthroscopic surgery has the benefits of reduced morbidity, less postoperative stiffness, and reduced recovery time [1, 2]. On the other hand, in open surgery the surgeon takes advantage of a wide field of view, and direct access to different parts of the joint is made possible through enlarging the incision made in the soft tissue. This is in contrast to minimally invasive surgeries, such as arthroscopic surgery, where access is limited to incisions and as a result direct view of the inside of joint is not available to the surgeon. In order to make manipulation of tools through small incisions possible two special tools are utilized. These tools allow visualization of the surgical tools within the joint. Firstly, an arthroscopic camera is inserted into the joint space through one of the incisions. Using this camera it is possible to view the interior of the joint, locate the site of damage, view the tool(s) inside the joint and position them in the correct orientation prior to starting the procedure. Secondly, a fluoroscopy unit in the form of a C-Arm is used externally to obtain fluoroscopic images of the joint after the

tools are placed inside the joint. These fluoroscopic images provide the information about the relative position of the surgical tools with respect to the site of interest within the joint. The additional advantage of the fluoroscopy unit in the form of a C-Arm is that it allows for imaging the subject at various angles. Therefore the spatial visualization of the tool is made much easier. The most common views obtained in surgery are antero-posterior (AP) view and lateral view.

Despite the different approaches in the open versus minimally invasive procedures, the overall functional improvement of the joint is comparable in both types [3]. Minimally invasive procedures have become popular in recent years mostly because of the advantages they offer over the open approach. Lower recovery time makes it possible for the patients to return to normal life style faster. Additionally, with faster discharge of patients postoperatively, hospitals will be able to accommodate more patients and provide health care services for a larger number of patients in a shorter period of time.

It is important to note that the minimally invasive nature of arthroscopic surgeries makes these procedures more prone to complications. Performing full inspection of the joint is more difficult in minimally invasive procedures and failure to do so can lead to an incomplete correction of the physiology. This in turn causes the joint to be unstable after operation [4, 5, 6]. Furthermore, sensitive structures such as soft tissue, nerves and major blood vessels are present within close vicinity of major joints. Therefore, an inaccurate approach to modifying the joint structure can cause harm to these structures leading to further complications such as deep-vein thrombosis, neuraparaxia, avascular necrosis, iatrogenic chondral damage, hetero-

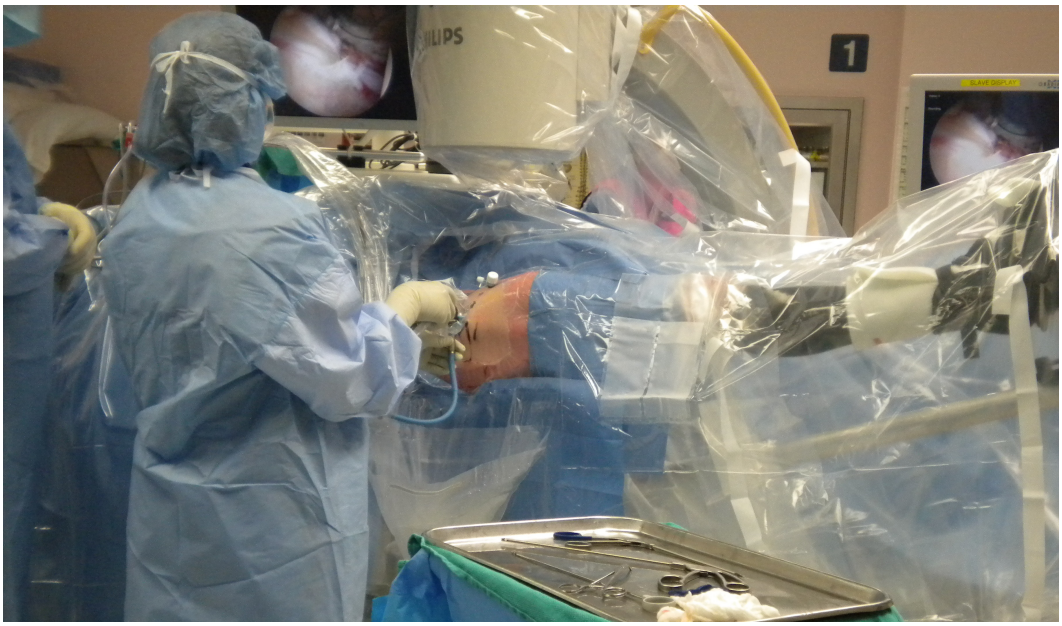

Figure 1.1: Hip arthroscopy setup (Courtesy, Dr. I. Wong, Dept. Surgery, Dalhousie University, Dec 2012).

topic ossification, and fracture of femoral neck [7].

Depending on the type of joint that is being operated on, complications of the procedures can be more or less serious. The shoulder joint (rotator cuff) is complex because of the number of tendons that insert around it; however it is quite superficial and as a result relatively easy to access. The knee joint, due mostly to sports injury, is most commonly operated on. The unique difficulty regarding this joint is the presence of the cruciate ligaments (anterior and posterior cruciate ligaments, commonly referred to as ACL and PCL) and the relative difficulty for accessing this joint at the site of interest. Finally, the hip is a commonly injured or merely worn joint, particularly in adults. The main complication faced when performing hip arthroscopy is due to the fact that it is a deep joint and depending on the size of

the patient, accessing it can be quite difficult.

1.1 Arthroscopic Surgery Training

The specific nature of minimally invasive surgery like arthroscopic surgery raises the requirement for extensive training in order to lower, and even eliminate, the chance of complications. While these procedures are becoming more popular for the reasons discussed before, a major factor presenting a challenge to new surgeons undertaking arthroscopic techniques is that these procedures are challenging, and technically quite demanding. However the correct performance of the procedure leads to a better evaluation and treatment of lesions in the joint through two or three very small incisions [8]. Therefore, by providing effective training for surgery residents, it is possible to provide better treatment for patients through arthroscopic surgery.

Classical training for arthroscopic surgeons have been based on learning by watching an experienced surgeon perform the procedure (the so-called apprenticeship method) [9, 10]. The cost of this kind of training is one of its significant drawbacks. In fact the cost of such methods of training have been estimated as high as $\$48,000$ per resident assuming four years of operative training before graduation [11]. Additionally, it is not always possible to provide the one-on-one opportunity for every resident and as a result they will have to learn the necessary skills in less than optimal operating room time [12, 13]. Patient safety throughout surgical procedures is an important factor to be considered. When learning through apprenticeship there

is a high risk of damaging the tissue and causing further problems for the patient. With the improvements in the computer and graphics engineering many new ideas have evolved for creating the operating room experience without the need to have a patient present. Since virtual training allows for error while learning, these systems have started to become quite popular in the field of minimally invasive surgery training.

1.1.1 Essential Components of Training

Arthroscopic surgery training includes development of special technical skills including dexterity and hand-eye coordination [14]. In order to provide effective training for arthroscopic surgery the training protocol must include aspects that help the residents develop and master these skills. Additionally, it is essential to create an environment that very closely mimics the real surgery settings.

Arthroscopic surgeons take advantage of a stereoscopic camera to view the inside of the joint in real-time throughout the procedure. The surgeon also has access to a fluoroscopy unit (a C-Arm) and therefore is able to obtain images of the joint at various angles throughout the surgery. These two imaging tools compensate for the lack of direct view of the joint in minimally invasive procedures. Working with these two components makes up the most challenging part of the procedure. An ideal training system would provide a sufficient and realistic opportunity for the trainees to experience navigation with a stereoscope, manipulate tools within the joint and without a direct view, and perform all tasks while looking at the images displayed on the screens. The training system must allow for development of fine

motor movement skills that can be transitioned into an actual surgery. Other aspects that need to be incorporated in training include realistic representation of the patient and the surgical tools and tool-holders.

1.1.2 Limitations of Current Training Systems

Despite the evidence currently supporting the effectiveness of the existing training systems, there are limitations associated with them that create hurdles in providing complete and effective training for surgical residents. Firstly, training systems are extremely expensive [11] and therefore medical school training programs often allocate one station for every group of students. This means the students will not receive the necessary exposure to the hands-on activities as desired to achieve their training needs and goals. Secondly, utilization of fluoroscopy units require involvement of radiology technicians, which on its own adds to the cost of training. Additionally, the utilization of a fluoroscopy unit during the training exposes the trainees as well as the staff to unnecessary X-ray exposure. The current training can be improved by lowering the cost and eliminating radiation exposure. By doing so trainees can be assigned separate stations and in this way they are provided a better opportunity to obtain practical experience. Ongoing improvements in image processing techniques has made it possible to create realistic virtual experiences for several different applications. In fact these techniques can be used in the case of arthroscopic surgery training in order to eliminate the need to have a fluoroscopy system. This will eliminate the radiation component of current training systems as well as the cost associated with the need to have radiology technicians in the

training.

1.2 Goals of This Research Project

In this work I propose a composite training station that takes advantage of a physical model to represent the patient realistically, while taking advantage of image processing techniques to create virtual reality representing the X-ray fluoroscopy images of interest for the surgeon in training.

The virtual reality portion of the project takes advantage of previously obtained computed tomography (CT) images of a joint model as well as the surgical tools. By processing the 3D CT data it is possible to obtain an X-ray-like image of the object. This procedure is repeated to create an image library, which can eliminate the need for a fluoroscopy C-Arm in training. The fluoroscopy imaging in surgery is performed to display the 2 dimensional spacial relationship between the surgical tool and the joint. In order to complete the creation of virtual fluoroscopy image, the images of the surgical tools are overlaid on top of the fluoroscopy images of the joint using a 2D registration algorithm. This 2D registration is made possible through 3D tracking of the tools in the field of work. Registration is performed to reference the different components of this training to a common coordinate frame. The two coordinate frames in this project include the frame of the virtual images of the surgical tools and the joint model, and the frame of the tracking system, which includes the physical joint model. By registering these coordinate frames it is possible to obtain the image coordinates corresponding to any point in the frame of

the tracking system. Therefore the position of the surgical tools can be identified in real-time and, by applying the necessary registration transformation, the corresponding position in the virtual image of the joint model can be calculated.

The remainder of this thesis is organized as follows; in Chapter 2 a brief review of literature is presented to introduce arthroscopic surgery in more depth, and compare the different technologies available that can assist in designing an effective training system to prepare surgery residents for entering practice. Chapter 3 presents the detailed design of this novel training system. In Chapter 4 the results of performance analysis of the system is presented. Chapter 5 is dedicated to discussion and declaration of future directions for this project.

CHAPTER 2

Background

Effective training in arthroscopic surgery is crucial in improving the quality of care delivered to patients. This includes a complete and effective repair of the joint, without incurring any damage to the joint and its surrounding tissues. This is particularly of interest in arthroscopic surgery, because the minimally invasive nature of the procedure makes it more likely for the surgeons to make error and cause damage to the joint. Current training systems incorporate a variety of technologies available in the fields of computer science and image processing as well as physical models to create the experience of operating room for the residents in training. There has been a number of published studies [15, 16, 17] on the outcome of using training systems to prepare the residents for an actual surgery. Despite the variety in the conclusions made by each of these studies, the common aspect of them is that they all consider the outcome of using these systems to be a significant improvement in the performance of new surgeons in the operating room. A number of shortcomings of the existing training systems leaves lots of room for improvement. This work proposes a novel approach for the integration of a number of available techniques and technologies to improve the quality of training delivered to surgical trainees.

This chapter starts by providing a detailed background on arthroscopic surgery and presents the current training systems. In section 2.1 of this chapter a detailed background on arthroscopic surgery is presented. Section 2.2 presents the available technologies that can assist in creating an effective training environment for this type of surgery. Section 2.3 of this chapter presents different registration techniques and concludes by a discussion of common approaches in solving for the registration parameters.

2.1 Arthroscopic Surgery

From a mechanical perspective, the motion of any joint in a structure is made efficient through careful design of the articulating surface. Ideally, a friction-free surface is desired to minimize wear and energy consumption for the motion of the joint. In human anatomy, all the joints in the body are surfaced with articulating cartilage, which allows for easy motion of the articulating bony structures that make up the joint. While the health of this structure is key to functionality of the joint, any damage to it can be a cause of progressive issues. This is because the articular cartilage does not have intrinsic ability to repair itself and as a result any instability or damage to it or to its surrounding supporting structures can lead to early arthritis [18].

The reasons for discomfort in the joint can vary from sports injury, trauma, or simple wear. Therefore the problem is not specific to elderly and as a result it is important to identify solutions to correct the range of motion of the joint and restore its

functionality in order to prevent development of osteoarthritis (OA) at a young age.

2.1.1 Surgery Setup

Arthroscopic surgery is performed by inserting surgical tools and a stereoscopic camera into the joint space. Through manipulation of these tools from the external environment modifications are made within the joint. While the stereoscopic camera inserted into the joint provides a direct view into the joint space, a fluoroscopy unit is utilized to obtain a better understanding of the spatial relationship of the the tools within the joint. These two tools greatly contribute in facilitating the performance of the procedure. Arthroscopic surgery is performed by a surgeon who looks at a number of monitors, which display the video from stereoscope and the images obtained from the fluoroscopy unit. Therefore performance of this procedure requires mastering hand and eye coordination.

Arthroscopic surgery is performed on various joints including the shoulder, the knee, and the hip joints. In each of these procedures the patient is prepared in a way that only a small area of the joint is exposed and the rest of the body is covered with sterile sheets. Depending on the joint being operated on and the level of repair needed for that joint two or three very small incisions are made through the skin in order to allow for insertion of surgical instruments. Figures 2.1- 2.3 illustrate the setup of this procedure for the shoulder, the knee, and the hip joints.

In the shoulder joint the cause of discomfort can be due to sports injury or trauma leading to tearing of the rotator cuff tendons and ligaments. Impingement is also a cause of discomfort for patients. This occurs when the humerus (the long bone of

Figure 2.1: Patient prepared for shoulder arthroscopy (Courtesy, Dr. I. Wong, Dept. Surgery, Dalhousie University, Dec 2012).

the arm) articulates directly with the rim of the glenoid (the shallow depression on the lateral face of the scapula) and often is because the cartilage is damaged allowing for this direct articulation. Arthroscopy procedures are performed to reattached the torn cartilage and the tendons allowing for the natural range of motion of the joint.

The knee joint is mostly damaged in sport activities such as soccer. Trauma causing this joint to bend in lateral directions can cause the tearing of ACL and/or PCL. Arthroscopic surgery is performed on the knee joint often to reattach the torn ACL/PCL. Due to the crossing of these ligaments this particular type of procedure is quite difficult and precise hand and eye coordination is required in order to avoid any further damage to the menisci. This is also the case in shoulder arthroscopy

Figure 2.2: Patient prepared for knee arthroscopy (Courtesy, Dr. I. Wong, Dept. Surgery, Dalhousie University, Dec 2012).

since this joint is quite small while multiple ligaments and tendons insert around it.

Hip arthroscopy is most often performed to address the discomfort caused by femoroacetabular impingement (FAI). This condition occurs when the normal anatomy of the hip is altered causing lesions to the cartilage and/or labrum [19, 20, 21, 22, 23]. FAI has been shown to cause OA of the hip [22]. Depending on the site of abnormal morphology, FAI can be one of three types; cam, pincer, or a mixed type [2]. In cam impingement, the anterolateral femoral neck has a rough articulation with the acetabular rim during movements such as flexion and internal rotation. This causes the labral-chondral complex to get damaged [24]. In pincer impingement the issue is on the acetabular side, which has an overcoverage of the femoral head-neck re-

Figure 2.3: Patient prepared for hip arthroscopy (Courtesy, Dr. I. Wong, Dept. Surgery, Dalhousie University, Dec 2012).

gion and labrum [25, 26]. This morphology constrains the normal range of motion of the joint. The morphology of normal hip joint and cam, pincer, and mixed types impingements are illustrated in figure 2.4.

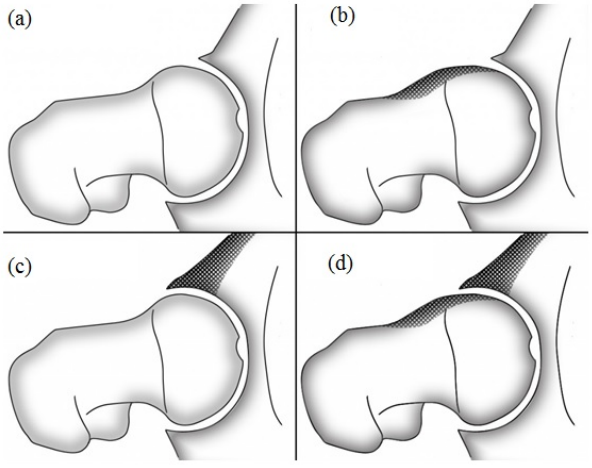

Figure 2.4: (a) Normal hip joint, and (b) cam, (c) pincer, (d) mixed type femoroacetabular impingement. Adapted from [27].

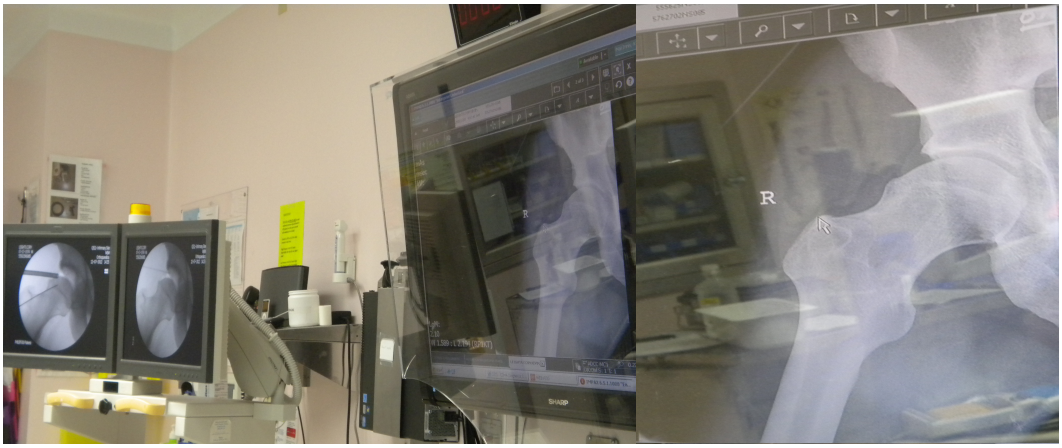

(a) (b)

Figure 2.5: (a) X-ray image and the fluoroscopy images, and (b) X-ray image, displayed throughout the surgery (Courtesy, Dr. I. Wong, Dept. Surgery, Dalhousie University, Dec 2012).

Preoperative X-ray images assist the surgeon in planning the treatment. Particularly of importance is the identification of all the regions that are causes of patient discomfort. These images are displayed throughout the surgery to ensure an effective treatment is delivered. The fluoroscopy unit is positioned such that it can capture the region of the joint with the tools inserted into it. Sometimes, the use of fluoroscopy unit is omitted in shoulder and knee arthroscopy, since these joints are superficial and easy to access. For these joints, omitting the use of fluoroscopy depends on the surgeon's preference and comfort with manipulating the tools inside the joint. In the case of hip arthroscopy, however, it is rather difficult to ensure the tools are positioned in correct orientation and at the right spot within the joint. This is because hip is a deep joint and access to it requires higher level of expertise and experience. Therefore, it is often preferred to use fluoroscopy to monitor the

location and orientation of the tools. It can be expected that in the case of hip, as the size of the joint is quite larger than other joints in the body, rotating the C-Arm to obtain fluoroscopy images at various angles is rather difficult. In addition to the larger size of the hip joint, the bed where the patient is positioned on and all its relevant equipments add to the bulkiness of the region that is placed in the imaging field of the C-Arm. Therefore, the C-Arm is usually used to obtain antero-posterior and sometimes lateral images.

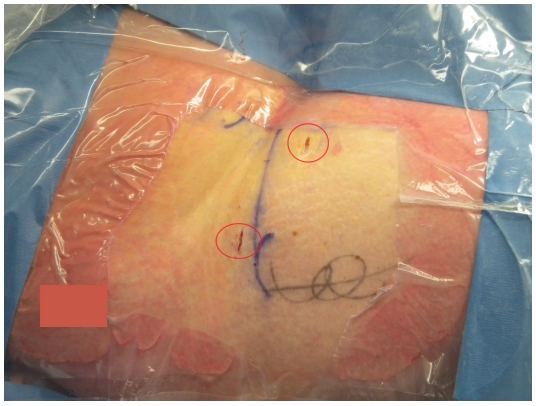

Figure 2.6: Access to joint made through small incisions on the surface (Courtesy, Dr. I. Wong, Dept. Surgery, Dalhousie University, Dec 2012).

An advantage of arthroscopic surgery is the minimally invasive nature of this procedure. While in open surgery the access to the joint is made possible by opening up the region, in arthroscopic surgery access to the joint is achieved through two or three very small incisions on the surface of the skin (Figure 2.6). This decreases the recovery time making it possible for the patient to return to normal life style faster and the hospital to accommodate more patients in less time.

2.1.2 Current Training Systems

Learning arthroscopic surgery skills through apprenticeship often leads to insufficient training and can cause potential iatrogenic injury to the patient [7]. Aside from the traditional fellowship learning, some schools use cadaveric specimens for training their residents [14]. This approach is very costly, labor-intensive, and of course requires such specimens to be available. Other options are utilization of anatomical models as well as simulated models [28, 10], which have the advantage of providing a way to quantify performance improvements while providing a close to reality learning experience. However, these systems are often costly [29].

Depending on the way the patient is represented in training, the system can be classified as physical, or virtual training. In a physical training system, as the name implies, a physical model of the joint is developed to closely mimic the characteristics of actual tissue. Actual surgical tools are utilized to manipulate the joint and perform a practice surgery. The downside of physical training systems is that they require a C-Arm to be utilized in the session and consequently one or more radiology technicians must be included as part of the training staff. This adds to the cost of training and increases the number of resources needed. In order to address this shortcoming of physical systems, virtual systems have been designed. Virtual reality (VR) is the generic name given to technologies that create a virtual perception of a certain task without the need to include the actual physical components. A number of VR systems have been developed and tested [9, 14, 30, 31, 16, 28, 32, 33, 29, 34, 15, 35]. In all these studies it has been successfully shown that training with virtual systems leads to improved per-

formance in surgical techniques. Some studies also considered the translation of skills learned through such systems to the operating room [17, 16, 15, 14]. These studies conclude that training with VR systems has significant improvement in the process of skills translation to actual surgery. In a virtual system, the patient or the joint is a virtual model that can be viewed on the screen of a computer. Tools are represented by joystick-like manipulators that are interfaced with the computer. Motions performed by the trainee are translated into 3D images on the screen. The major requirements of virtual training is to include haptic feedback in the system. It is important that the trainees be able to know how much pressure they need to apply and whether they are within the joint capsule and at the correct position, therefore incorporation of realistic haptic feedback is an essential part of virtual training [36]. However, lack of realism is still a concern in the existing training systems [37] and therefore the utilization of physical models of the joints can be quite beneficial in the process of training.

2.2 Virtual Reality and Tracking

With the increase in the application of computers in various fields, the need to design and develop accurate and reliable interfaces between them and their external world also raises. This interface, in one way or another, is created through tracking the objects in the external world and transferring the information about their position and orientation to the software in order to enable them to perform the subsequent tasks.

Medical interventions, particularly minimally invasive surgeries, take advantage of tracking systems in order to deliver safer and better treatment to the patients. The involvement of machines while keeping the physician as the final decision maker is essential because, while computerized processes can make the delivery of treatment much more accurate, the critical decision-making ability of the doctors make them an important part of the task.

Traditionally VR systems interfaced with a computer by tracking the head or eye movements through use of a head-mounted display (HMD) [38], however improvements in the system has made it possible to include motion of hands, arms and complete body. One of the recent applications of VR is in surgical training where its utilization has been shown to significantly improve the performance of the surgeons in the operating room [15, 10, 39]. VR is also used in medical planning, as well as rehabilitation and psychiatric therapy [40, 41]. Virtual reality has been used for aviation training where, instead of allowing a new pilot to participate in an unsafe training such as flying an actual plane, the experience of flight is simulated in a computer (aircraft simulator) [17]. In addition to aviation training, VR has been used to replace “on-the-job-training" (OJT), for delivering a more effective training of the flight maintenance crew [42]. Such technologies often take advantage of tracking systems to allow for creating the interface between computers and external objects. Tracking systems have other applications than VR. Study of human motion and gait, for example, takes advantage of tracking systems, most often optical systems [43, 44]. Regardless of the specific application, tracking systems serve the common purpose of keeping the position and orientation of the objects known to

the central processing unit.

2.2.1 Tracking Systems

In a tracking system a coordinate frame is assigned to each of the two main components of the system; the source and the sensor. A third component, the data acquisition unit, is necessary to process the raw data and calculate the position and orientation information. These components are common among different tracking modalities. Additionally, depending on the setup of the system, trackers can be active or passive systems. In both types of systems the sensor is attached to the object being tracked. Whereas in active systems there is active communication between the sensor and the source, the passive systems do not produce any communicating signals to the source [45]. While manufacturers supply accuracy and resolution data with their products, the validity of tracking systems mostly depends on the application. It is good practice to test the tracking system in order to establish the application-specific resolution and accuracy [46].

Tracking devices commonly used are usually one of four types; mechanical tracking systems (MTS), optical (OTS), acoustic/ultrasonic (UTS), or electromagnetic (EMTS). To evaluate the position and orientation information, MTS use the direct connections between mechanical parts, OTS take advantage of a camera system and special markers, UTS utilize phase differences in signals transmitted and received, and finally EMTS use the coupling between the transmitted and received signals.

2.2.1.1 Mechanical Tracking Systems

Mechanical trackers are considered the most reliable tracking systems as their method of calculating position and orientation is least prone to error and interference [47]. Mechanical trackers are active systems and are made up of joints and links. Links are the separate arms that connect to each other at a joint, therefore for n joints there are $n + 1$ links. At each joint there is an encoder that measures the relative angle between the links connected to that joint. This layout of mechanical systems is the main reason for their use in most sensitive tracking applications. The physical joining of each link leaves very little room for error so long as the sensors measuring the joint angles are accurate [47]. A relationship can be derived relating the lengths of each link and angles between the subsequent links to calculate the position and orientation of the end-effector (the tip of the final link) [47, 48].

Mechanical trackers can be one of two types depending on the type of joints that connect the links. These joints can be prismatic or revolute. Revolute joints allow rotation of the joint about a single axis, while prismatic joints allow the sliding of the two links making up the joint [49]. As long as the joints are purely revolute, the only factor that changes is their orientation. If the joints are prismatic, then the offset between two subsequent joints also varies.

In utilizing mechanical trackers n links need be considered and for each link a unique coordinate frame needs to be assigned. These frames are assigned based on a convention, the most common one of which is the Denavit-Hartenberg convention [49].

In order to go from base frame to the end-effector frame, each of these coordi-

Figure 2.7: Mechanical tracking system (Phantom by SensAble Technologies).

nate frames must be rotated and translated. The result of these transformations is a matrix, which is a function of joint variables (the angles at each joint and the lengths of the links). Mechanical systems, sometimes referred to as spatial linkage systems [48], were the first tracking systems to be incorporated into image-guided surgery and particularly for cranial procedures. Stereotaxic procedures take advantage of this type of systems to register the patient at the time of surgery to preoperative images and to finally help the surgeon guide the tools to the site of interest within the patient's body. The major disadvantage of these systems is that they are usually bulky and therefore it is rather difficult to incorporate them into most surgery settings. Furthermore, attachment of a surgical tool to the end-effector of a mechanical system limits the freedom of motion and this is not always tolerated in surgical procedures.

2.2.1.2 Optical Tracking Systems

Optical tracking systems are most commonly used in surgical as well as biomechanical applications. Study of gait, often involve motion capture, where using the combination of a camera and a number of optical markers, the motion of the joints is tracked. Optical systems are popular because they have good accuracy with large working volumes [48]. In surgical applications the optical sensor is often positioned at a certain distance from the tip of the tool, which itself is what is being tracked. The accuracy of the optical-based tracking systems can be as good as submillimeter [46, 50], and this gives the accuracy of detection and tracking for the tip of the surgical tool in the range of $1 - 2$ mm, which is acceptable in most applications. However, it is rather difficult to obtain stable orientation measurements with a limited number of markers that are located in close proximity to one another. Depending on the application an efficient design for the placement of the markers should be obtained to ensure system performance is acceptable. Another, more limiting downside of these systems is that optical trackers are line-of-sight systems, which means one must ensure that the markers used are always in the line of view of the camera. As a result the utilization of this type of tracking technology is difficult in the crowded condition of an operating room [51]. This can be overcome by using multiple cameras in the system to add redundancy, however designing a multi-camera system not only adds to the already high cost of the system, but also makes transportation of the system difficult. Aside from these, optical systems also rely highly on the assumption that the object being tracked is rigid. Even the slightest bending of the object can lead to large enough error producing invalid position

and orientation output [48].

(a) (b)

Figure 2.8: (a) Passive, and (b) active optical tracking system (NDI, Waterloo, Ontario).

The three main components of OTS are the camera, markers, and the processing unit. Optical trackers are either active or passive systems (Figure 2.8). Active trackers make use of infrared-emitting markers. The camera detects these markers and the processing unit is able to calculate the position and orientation information of the object being tracked. These markers are activated by electrical signals. In passive optical tracking systems, spherical, retro-reflective markers are used. These markers reflect the infrared light that is emitted by the illuminators positioned around the camera. The reflected light is then detected by the camera and the processing unit calculates the position and orientation of the object being tracked [48]. In addition there are systems that can adapt to both active and passive configurations.

2.2.1.3 Ultrasonic Tracking Systems

Ultrasound imaging is commonly used in surgeries to guide instruments into the target tissue. This modality of imaging is usually preferred over X-ray and CT imaging as it does not cause radiation exposure, is relatively cheap and can be readily available throughout the surgery. Ultrasonic tracking systems include similar advantages. Such systems usually include a transmitting unit and a drive unit. The transmitting unit is attached to the object being tracked and works by producing brief periodic acoustic waves. The drive unit includes a receiver. In ultrasonic-optic hybrid systems, the drive unit also includes a motorized component that controls the orientation of its camera. The receiver is capable of producing control signals in response to the time differences at which its microphones receive signals from the transmitter. These controlling signals direct the motion of the motorized component to ensure the receiver and/or the camera are always pointing towards the object being tracked [52]. The limiting factor for this class of trackers is the issues that may be caused by interference of ambient sounds and even temperature fluctuations in the surrounding environment [48]. This leads to the need for frequent re-calibration of the system.

2.2.1.4 Electromagnetic Tracking Systems

EMTS are considered one of the older technologies; however, the improvements in the accuracy and performance of these systems have made their application in variety of fields possible [48]. These systems are based on electromagnetic waves generated and emitted by a source and the reflected electromagnetic wave by a sen-

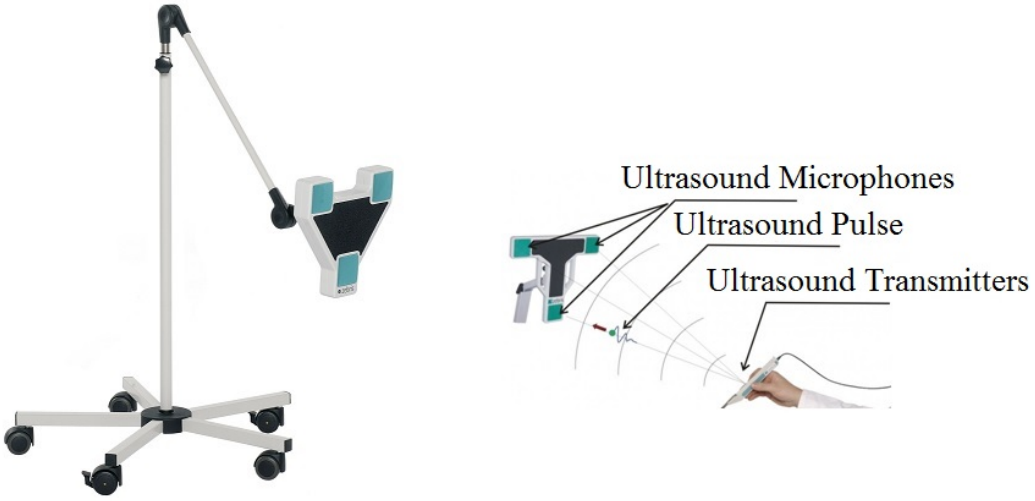

Figure 2.9: Ultrasonic tracking system (Zebris Medical GmbH, Isny im Allgau, Germany).

sor. All electromagnetic tracking systems consist of same general components; the field generator or the source, the sensor(s), and a main electronic unit that performs the synchronization between the two and the calculations of the position and orientation of the sensor with respect to the source. The source and sensor both consist of three orthogonal coils, which are in ranges of 0.5 mm to 1 mm in diameter and 5 mm to 10 mm in length. EMTS sensor coils are able to resolve translation and orientation in two planes of pitch and yaw. However in order to compute the total of 6 degree of freedom, two or more coils must be combined. This can also be achieved by using dual-dimensional winding [48]. Having three coils in the field generator and three coils in the sensor is most reliable and common configuration (the so-called 3-by-3 configuration) [53].

(a)

Figure 2.10: Electromagnetic tracking system (Polhemus, Colchester, VT).

EMTS can also be subdivided into active and passive systems. In active systems the sensor is connected to the tracking system by wires. Passive systems are wireless and take advantage of radiofrequency (RF) technology to power the sensor through a pulse of electromagnetic energy. Passive systems are not as commonly manufactured or used because their wireless nature leads to a lower range of functionality as well as lower accuracy [48].

Electromagnetic fields are generated due to the current running in the three orthogonal loops of wire. Depending on the type of current running through the tracking system's coils there are two different types of electromagnetic tracking systems. One system uses alternating current (AC), while the other uses direct current (DC). AC systems output their signals on a high frequency carrier wave and the amplitude of the signal received is used to calculate the position and orientation information. DC systems generate a quasi-static field in a particular excitation pattern. Each excitation in the field generator's coils produces an excitation vector, which further leads to a response from the sensor. The output vectors from the sensor has information that can be used to calculate both position and orientation of the sensor in

the frame of the field generator[54]. It is a significant requirement of DC systems to delay position and orientation computation until the transient response signals have died out. The advantage of an AC electromagnetic tracking system is that it utilizes current at different frequencies and therefore simultaneous collection of data for X-, Y- and Z-coordinates of sensor is possible. This is while in DC-based systems each of the axis coils need to be triggered separately and also a delay needs to be added in order to avoid interference [47, 53]. Therefore, using AC-based electromagnetic systems speeds up the tracking considerably.

The main problem concerning EMTS is that the presence of metal objects in the electromagnetic field can cause major interference. Particularly the older systems were quite susceptible to magnetic interference and as a result electromagnetic-based trackers are not as popular as optical systems [48]. However, newer systems that have been improved, are capable of resisting interference for small metal objects. It is noteworthy here that in newer EM-based trackers, only large metal devices, in the size-range of a C-Arm, have been shown to negatively affect the system [55]. As a result these systems can be quite useful in applications where such large metal parts can be eliminated from the field.

The important benefit of electromagnetic trackers is that their functionality is not dependent on a clear line-of-sight and this gives them advantage over the optical systems. Very small electromagnetic sensors can be placed close to or at the tip of the tool making it possible to track the tip directly. Therefore, in some cases the potential of interference in EMTS is compensated for by this capability. Similar to optical systems, the advantage of using EMTS compared to MTS is the freedom of

motion of the tracked objects within the field of operation of the system.

2.2.1.5 A Comparison of Available Tracking Systems

In considering different tracking systems the advantages and disadvantages of each of the systems can be considered important or insignificant depending on the application at hand. Mechanical trackers are most accurate systems. However, they are bulky and do not allow the freedom of motion as much as the other available systems. Ultrasonic systems are not very popular because of the lower resolution and the fact that they are highly prone to interference from the different sources including the temperature of the surroundings [48]. Ultrasonic systems became less used in various applications with rise in the production of high accuracy optical systems. Optical systems can offer excellent tracking accuracy and a large volume of work. Nonetheless, they are usually costly because of the high resolution camera component. In addition, optical systems have the line-of-sight constraint and as a result they can cause issues in a cluttered surgery setting [55]. Lastly, the new electromagnetic tracking systems are capable of reaching a very good accuracy and they have the advantage over the optical systems in that they do not require a clear line-of-sight and as such direct tracking of the tip of the tool using EMTS is quite possible. However, these systems are susceptible to interference in presence of metallic objects. The accuracy and performance of optical systems and electromagnetic systems have been compared and similar results have been reported for both [56]. Nevertheless, one cannot make the generalization, as the accuracy achieved by these systems and their susceptibility to interference varies greatly de-

pending on the application [47].

One main contributor to the inaccuracies encountered in all tracking systems is the progressive error that is due to distance between the end-effector, sensor or marker being tracked and the point of interest on the object. It is not always possible to position the sensor at the point of interest. For example in tracking surgical tools within the field of work it is not quite possible to position the sensor at the tip of the tool. The sensor is often placed a certain distance from the tip and, knowing the position and the orientation of the sensor, the position of the tip of the tool is calculated. However, the error in calculating the position of the tip is very much affected by the error in identifying the position and orientation of the sensor. This error is related to the distance between the sensor and the point of interest, and the angle of rotation through the following relationship:

$$\varepsilon_i = d_{tip}.\delta_i \tag{2.1}$$

where ε_i is the error at the tip of the tool at the i^{th} measure, d_{tip} is the distance between the sensor to the tip of the tool, and δ_i is the error in the calculation of the orientation angle at the i^{th} measurement [46]. Therefore it can be predicted that as the distance, d_{tip}, increases the error in locating the tip of the tool also increases.

Aside from resolution and accuracy, cost is a factor that is often considered to determine the feasibility of a tracking system for particular application. While mechanical trackers are capable of returning high resolution position/orientation information, they are usually very expensive. Optical system can be as expensive if its

camera component is a high resolution camera. These systems can be even more expensive when the system consists of multiple cameras to make possible the depth perception in the process of tracking. Electromagnetic trackers can also be quite expensive depending on the size and number of sensors, accuracy of detection as well as resistivity to interference. Ultrasonic systems are probably the cheapest systems available, however, they too vary in cost depending on their resolution and number of detectors.

Table 2.1: Comparison of Different Tracking Systems

Tracking System	Resolution	Cost
MTS	0.007 - 0.03 mm 0.0023°	Mentis (Xitac ITP) $31,500 [57]
OTS	0.25 - 0.30 mm at 2400 - 3000 mm range	NDI(Hybrid*): $19,450-$22,550 NDI(Passive): $11,500 [58]
UTS	0.01 - 0.1 mm at 1 - 2 m range	Zebris CMS10 (6 sensors): $8,856 [59]
EMTS	0.0038 mm at 300 mm range, 0.1° orientation	NDI: $15,650-$17,900 [58], Can be moderate at the expense of sensor size; Polhemus: $3,550 [60]

* Passive and active together

Table 2.1 summarizes the tracking systems and their associated accuracy and cost factors. It can be concluded that for many applications there is no one tracking modality that works perfectly. Given the restricting factors such as presence of metallic objects in the field of work or the crowded nature of the environment for certain applications, it is sometimes necessary to build redundancies or combine multiple tracking modalities to obtain the resolution necessary. Some groups

have looked into calibrating EMTS using OTS in order to create a reliable system and accurate position and orientation readings [51, 61]. Much like image fusion, where anatomical and functional information can be obtained using multiple imaging modalities, the hybrid tracking systems can lead to high resolution readings and reliability.

2.3 Registration

Any object in space can be assigned a reference frame and the position and orientation of this object can be describe in this coordinate frame. For example, when medical images of a patient are taken an image coordinate frame is associated with the image data. When a patient is in a surgery room, the image data can be used to help in the surgical procedure. The patient is assigned a coordinate frame, sometimes termed "physical" or "world" coordinate frame. In order to match these different environments, the image reference frame and the world reference frame, there is a need to match the dataset obtained from each coordinate frame. Registration is the process of transforming data from one coordinate frame into the other.

Once a coordinate frame is defined, all the points of interest can be assigned X-, Y-, and Z-coordinates with respect to this base frame. In simple words, the base frame is assigned and all subsequent measurements and computations for position and orientation are performed with respect to it. The parameters that are needed in order to represent the position of an object as well as its orientation are referred to as the transformation parameters. Registration is often performed using fiducial

markers [62, 63]. These are either landmarks that are easily identifiable on images, or physical markers that are visible on the image. For mapping the dataset, firstly the coordinates of each of these fiducial markers is obtained in the image coordinate frame. Secondly, using a tracking system the coordinates of those fiducial markers are identified in the physical coordinate frame. The two sets of points are used to construct a system of equations where the unknowns are the transformation parameters between the two coordinate frames.

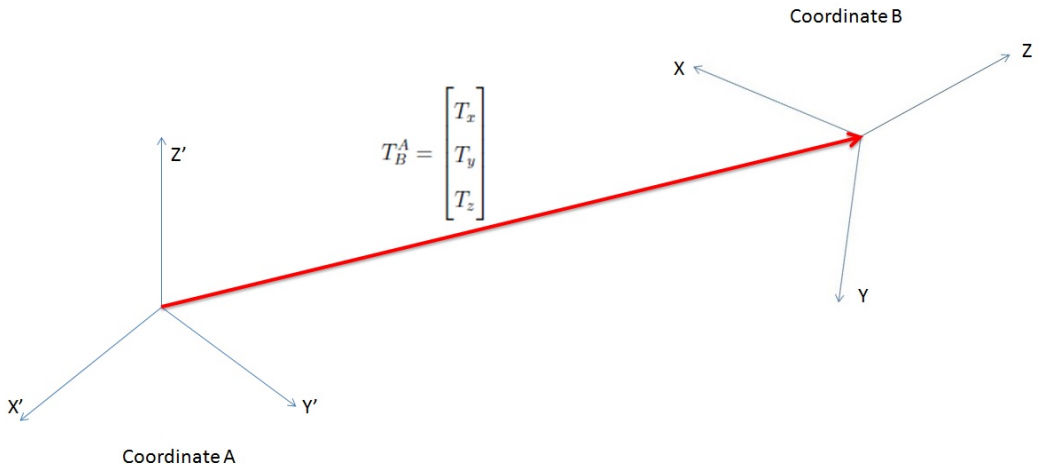

Figure 2.11: Representation of conversion between two coordinate frames.

The simplest way to setup the registration parameters is to separate them in a rotation and a translation set. As the name suggests the rotation parameters represent the various rotations that are necessary to go from the base coordinate frame to that of the object and the translation parameters represent the translations along X-, Y- and Z-coordinate axis in order to align the position of the rotated frame with that of the object. There are 9 rotation parameters that are commonly put together to form a 3-by-3 matrix (Equation 2.2). The translation parameters are 3, since translation

needs to be expressed in terms of the three axis; these parameters are put together in the form of a vector (Figure 2.11). The rotation matrix is multiplied with the co-ordinates of the point in order to find the effect of rotation on all three coordinates, and the translation vector is added to it in order to offset each of the coordinate axis in its corresponding direction.

$$R_B^A = \begin{bmatrix} R_{11} & R_{12} & R_{13} \\ R_{21} & R_{22} & R_{23} \\ R_{31} & R_{32} & R_{33} \end{bmatrix} \tag{2.2}$$

The process of registration is based on the fact that any object in one coordinate frame can be transformed to another frame by a series of rotations and translation. In a Cartesian coordinate frame the rotation can be about each of the axis, X-, Y-, Z-axis and in any order. Rotation about the X-axis is referred to as Roll (often denoted by the Greek letter ϕ), rotation about the Y-axis is referred to as Elevation or Pitch (denoted by the Greek letter θ), and rotation about the Z-axis is referred to as Yaw (denoted by the Greek letter ψ). The representation of these angles is illustrated in Figure 2.12. Each of these rotations is described in a 3-by-3 matrix and by multiplying them in a specified order it is possible to describe the orientation of the object. Different systems have unique specifications regarding this order for the rotations. For instance, the Polhemus Patriot (Figure 2.10 Polhemus Colchester, VT) specifies the order Yaw-Pitch-Roll. Failure to follow this order can lead to incorrect description of position and orientation of the object.

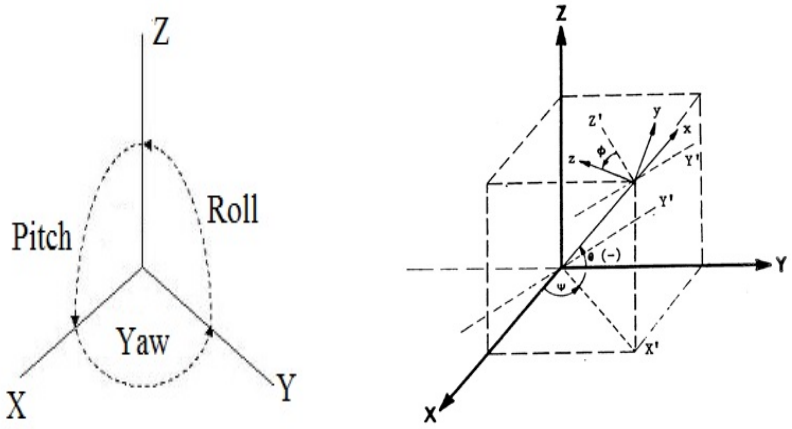

Figure 2.12: (a) Roll, pitch, and Yaw angles, (b) description of object orientation in space(Polhemus).

2.3.1 Image Registration

Image guidance has been utilized for quite some time to assist surgeons in achieving a higher accuracy and a better result from surgical procedures. This intervention is widely used in neurosurgery, orthopedic, and other such surgical procedures where the target organs can be assumed rigid and their spatial relationship to the anatomical landmarks can be thought to remain constant. In general surgery, organ shift always happens which makes the navigation using pre-operative images rather difficult. It is noteworthy that even in neurosurgery, sometimes the shift in organ, more often the inflammation in the brain tissue, is also considered significant and utilization of pre-operative images does not lead to an accurate navigation [64, 65, 66, 67].

Image registration is the process of matching the data found in different images of

(a) (b)

(c)

Figure 2.13: 2 dimensional image registration (a) complete image, (b) part of the original image, (c) registered and superimposed images.

the same object into one single frame of reference. Image registration generally consists of a number of steps. Firstly it is necessary to be able to detect common features on the images. This feature needs to be easily and reliably identified on the multiple images that are being registered. The process of feature selection can be either automatic through use of software or manual. Next these features must

be matched and a geometric transformation inferred. Finally using this geometric transformation one image can be aligned with the other [68]. This process is illustrated in Figure 2.13. Figure 2.13a shows the a complete branch of a tree with red and white blossoms. Figure 2.13b shows a black-and-white section of this branch. Using pronounced features in the two images, such as the corners of small sub-branches that are coming out of the main branch and the edges of the blossoms, it is possible to identify the corresponding points in the two images. Once these features are identified the 2 dimensional registration can be performed and the two figures can be overlayed on top of one another. This co-registered image is shown in Figure 2.13c.

2.3.2 Coordinate Frame Registration

Coordinate frame registration is the application of registration to objects whose coordinates are known in different base frames. Registration of coordinate frames can be either rigid or non-rigid. A rigid body is completely characterized in space by its position and orientation with respect to a frame of reference [49]. In rigid registration one assumes the objects are non-deformable whereas in non-rigid registration objects are deformable and as a result constant monitoring and updating of the system is necessary. The rigidity assumption makes calculations very much simpler. However, if the environment is not completely non-deformable, as is the case with most human tissue, the system calculations can become erroneous. In surgical procedures such as arthroscopic surgery, the tissue of interest, bone and cartilage, are assumed to be rigid, and as the surrounding soft tissue are not of major concern this

assumption is often acceptable.

The significance of having a rigid environment is because the level of accuracy achieved by the system is highly dependent on the registration performed at the start of procedure. This registration maps the object (usually the patient) as positioned throughout the surgical procedure to its position and orientation at the time of image acquisition pre- or intra-operatively. Depending on the type of tissue being operated on and the nature of surgery, the registration step can be performed using a rigid or non-rigid algorithm. Whereas rigid registration does not require periodic updating, non-rigid registration requires a way of accounting for the changes in tissue and compensating for that motion throughout the procedure. Therefore rigid registration is relatively simpler to perform.

2.3.3 Solving for Transformation Parameters

Registration makes up a significant stage of projects that are concerned with tracking and transforming information from one coordinate frame to another. There are a number of approaches available in finding the registration parameters [69]. Generally in 3 dimensions there are 12 unknown position and orientation parameters. As a result a minimum of 12 equations are required to perform the registration. In other words, the coordinates of 4 points (at least) from each of the two frames need be known in order to find the registration parameters.

While setting up a system of 12 equations for 12 unknowns can give an exact solution, sometimes this method is not desired. This is because the solution of this system of equation is an exact solution that fits the 12 unknown parameters per-

fectly. However, it could provide a poor estimate of the overall transformation. This could result in significant inaccuracies when applying the transformation to localized targets that were not used for registration. Therefore it is beneficial to utilize a more computationally intensive method that can give a more general and accurate result. The method of least square (LS) is a common method used for applications of data fitting. In this approach more equations than the number of unknowns are constructed (this is an overdetermined system); this means that there will not be a unique solution that fits all these equations. Instead, a set of parameters are identified that best fit the equations. One factor that must be considered in testing the result of registration using this approach is to ensure that the points used for registration are not points used for testing. The reason for this is that utilizing the LS method to find solution for the overdetermined system will lead to a best fit solution and while some of the points used to construct the initial equations may end up on this best fit function, others may not. Therefore, as long as the set of points used for registration are different from the points used in the testing, the method of least square gives better results for the registration.

Characterizing transformation and finding rotation parameters using Euler angles is the most common approach in coordinate frame registration. However, in some situations, this method leads to singularities, a solution that is not unique between two orientations that are mirror images of each other. This phenomenon is referred to as gimbal lock, and is the situation where the mathematical solution for orientation of the object is not unique or stable. Gimbal lock occurs in calculating rotation through Euler angles, when the second axis of rotation is at 90 degrees. As an ex-

ample, if a rotation of 90 degrees is performed about the Y-axis (pitch), the yaw and roll axes (Z and X axes, respectively) will become alighted. This change in the alignment of the rotational axes is illustrated in Figure 2.14. The result of this is the loss of one complete rotation, because a rotation about the X-axis, which normally causes roll, will also cause yaw.

Another mathematically involved and more accurate method of registration is

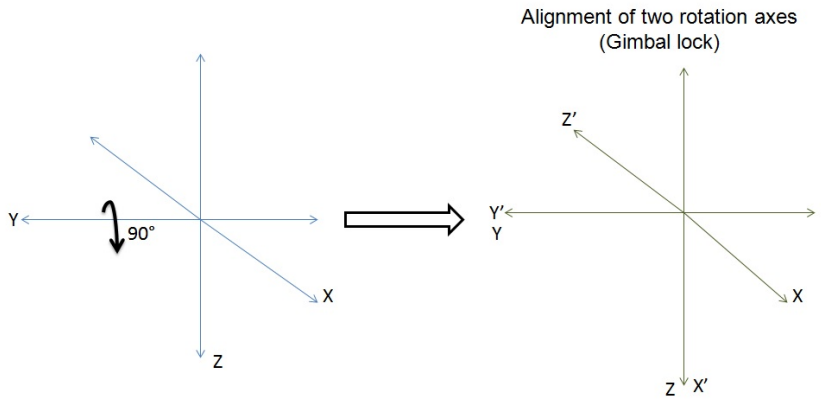

(a)

Figure 2.14: The phenomenon of gimbal lock.

through utilizing a vector and an angle to describe the orientation of an object in space. This method is called the "angle and axis" approach. In this method a vector component is defined in space that represents the translation of the object in the base frame (term $\overrightarrow{\varepsilon}$ in Equation 2.3) and a scalar term (term η in Equation 2.4), which represents the orientation of that axis in space.

$$\overrightarrow{\varepsilon} = \sin\frac{\theta}{2}.\overrightarrow{r} \tag{2.3}$$

$$\eta = \cos\frac{\theta}{2} \tag{2.4}$$

In Equation 2.3 the term $\overrightarrow{r}$ is the unit vector about which the rotation is taking place, and in both equations the term θ is the angle of rotation. This method is beneficial because it leads to definition of a unique solution for all possible orientations of the object. This means that by using the angle and axis approach it is possible to avoid the phenomenon of gimbal lock.

CHAPTER 3

Artificial Fluoroscopy System

The purpose of this project was to develop an artificial fluoroscopy system. This artificial fluoroscopy system is a virtual X-ray image display component combined with a physical joint model, which represents the patient. The primary priority in this project was to incorporate the essential components of arthroscopic surgery training into the developed training system. The following three characteristics were identified as important for the artificial fluoroscopy system:

1. The physical model should be capable of representing typical morphological abnormalities that are observed in the joint diseases, and further, these abnormalities must be reflected in the virtual fluoroscopy images.

2. The system must function in real time with minimal delay.

3. Physical interaction between the surgical trainee and the surgical tools and the patient model must be as close as possible to that in the operating room.

This product is aimed to create a realistic, low-cost, and radiation-free training system for arthroscopic surgery trainees. The virtual aspect of the system was created to eliminate X-ray exposure of the staff and residents, and additionally lower the

cost of training. The key goal for this training station was the real-time fluoroscopy image display without the use of an actual X-ray source/detector (C-Arm). In order to achieve this end result, a series of image processing techniques were customized to develop an image library. This image library was based on previously obtained computed tomography (CT) images of a joint model and as such identification of different joint morphologies were made possible. This would address the concern of item #1 in the above list. The 3 dimensional (3D) CT images were integrated and processed to create a 2 dimensional (2D) image database. As processing 2D images is much faster than handling 3D image dataset, using this image library it was possible to improve the speed of the system and design it so that its performance was close to that of an actual fluoroscopy unit. Therefore the goal identified by item #2 would be reached. Meanwhile, the physical joint model and the utilization of the actual surgical tools created a realistic training environment and therefore could make the transfer of skill sets from training sessions to the operating room more smooth. These aspects of the system address the concern in statement #3.

Image processing and 3D tracking make up the main components of this system. A flowchart representing the stages of the design and development in this project is illustrated in Figure 3.1. A physical joint model is used to represent the patient in the training system. The CT scan of this model is obtained and using several image processing techniques a library of 2D fluoroscopy images of the joint is created from the 3D CT data. CT images of the surgical tools are also converted into 2D fluoroscopy images. The surgical tools are tracked within the field of operation and by co-registering the image of the tool to that of the joint model it is possible to

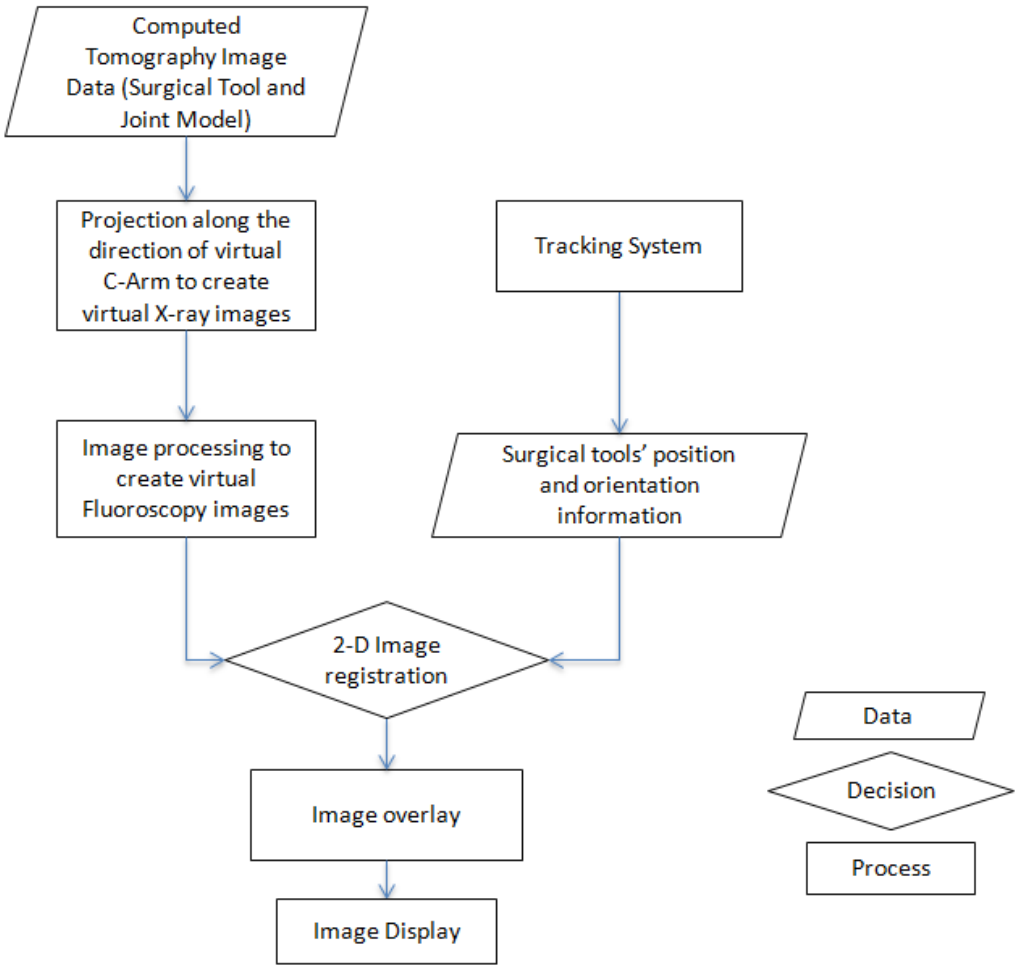

Figure 3.1: Flow chart for Artificial Fluoroscopy System development.

overlay the two, creating a complete fluoroscopy image of the site being operated on. This image will then be displayed for the surgical trainees giving them a visual representation of the relationship between the tools and the joint.

This project is organized into three main stages of development. Stage one of the project included a setup where the mechanical tracking system and a synthetic fe-

mur model were used to conduct a proof-of-concept experiment. In stage two the electromagnetic tracking system was used with a hip joint model, with the aim to increase the degree of free motion for the trainees and create a more realistic setup for the practice surgery. In the third and last stage of the project an image overlay algorithm was developed to create a realistic fluoroscopy image of the joint with the surgical tools. The present chapter is organized in a systematic fashion to present the various components of this project. In Section 3.1 a brief description of the two models that were used to represent the patient in this project is presented. Section 3.2 presents details on the virtual image creation of the joint. The virtual image creation of the surgical tool is presented in Section 3.3. The details on the two tracking systems used in this project are presented in Section 3.4. Section 3.5 of this chapter presents the details of the image overlay algorithm.

3.1 Physical Joint Model

Realistic representation of the patient was defined as a significant component of this training system. Additionally, a careful design of the joint model representing the patient can be an important contributor in lowering the cost of the training system. This can be achieved if the joint model is designed in such a way that some parts of it are re-usable and some key parts are replaceable to represent different joint pathologies. More specifically, during the surgery training, the only parts of the joint that are modified are the soft tissue and the joint space. Therefore, the model can be designed in such a way that these two portions can be removed and replaced.

Keeping the main frame of the joint model can reduce the cost of producing new models considerably, taking into account the number of models necessary for all the surgical residents.

DePuy Synthes Mitek Sports Medicine Inc. manufactures joint models that offer the desired features identified here. Figure 3.2 illustrates the hip joint model produced by this company. Figure 3.2a illustrates the complete model with the material that mimic the soft tissue. This material exhibits similar passive mechanical properties as muscle and can be pierced by surgical tools. Figure 3.2b shows the model with the soft tissue removed. The insert (see Figure 3.2d), which includes the proximal end of the femur and the acetabulum, can be removed and replaced after each practice procedure. Figure 3.2c and Figure 3.2d show the frame and the joint insert component of the joint model, respectively.

For the initial stage of this project a simple synthetic femur (Sawbones, Pacific Research Laboratories Inc.) was used (Figure 3.3). The goal in this step was to verify the concept of the system and therefore the consideration of the details of the joint model was not necessary.

3.2 Virtual Fluoroscopy Image Formation of the Joint Model

An X-ray image is created by transmitting X-ray beams through the patient, or any other objects. If the object being scanned consists of inhomogeneous parts, as is the case in human body, this transmission of X-ray beams will be weighted by the

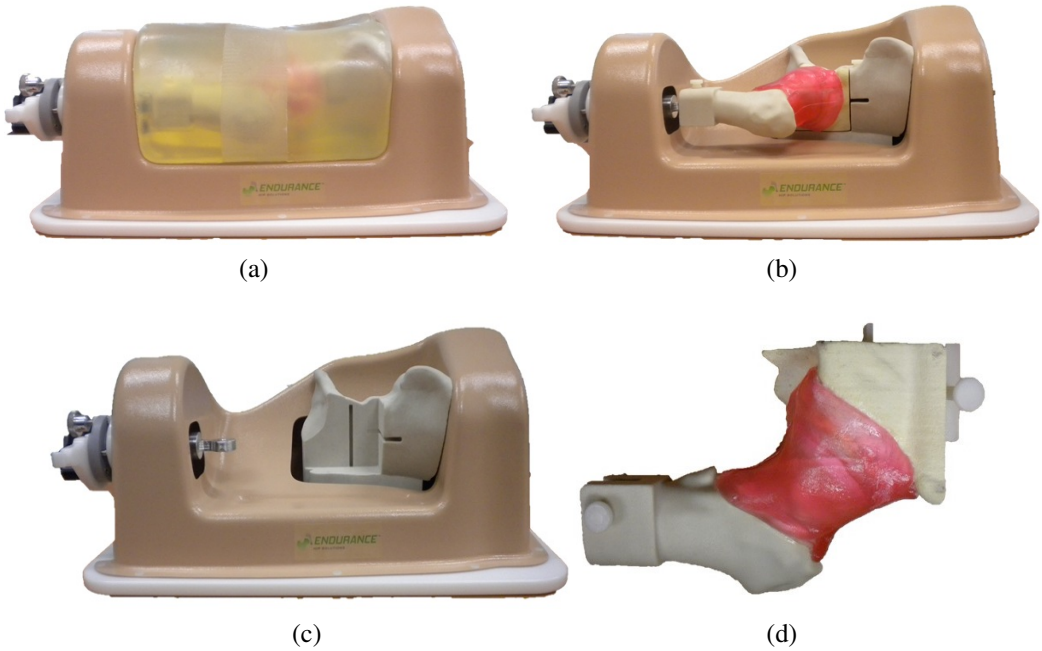

Figure 3.2: Hip joint model (a)with soft tissue intact, (b)without soft tissue(antero-posterior view), and(c)without soft tissue (lateral view).

Figure 3.3: Synthetic femur.

variable integration of loss of the beam energy. This loss is due to either scattering or absorption, which differ between tissues. An X-ray image is a 2 dimensional display of the transmitted beams [70]. In an X-ray image the higher intensities correspond to higher density regions (for example pixel values representing bone tissue

show as lighter, higher intensity) and lower intensities correspond to lower density regions (for example pixels that represent air have darker, lower intensity values). A CT scan is composed of a series of conventional X-ray image data. In CT imaging, however, the source and detectors rotate about the longitudinal axis (line connecting the head of the patient to the feet) between each exposure in order to obtain the projection at different angles around the object of interest. Therefore, a collection of horizontal lines contain data about one axial cross-section only. These projections can then be used to reconstruct a cross-sectional image [70, 71]. Repeating this technique over a longitudinal distance creates a final 3 dimensional image dataset that can be reconstructed into a three dimensional image. This process defines the routine CT scanning that is performed in a clinical setting. The intensity mapping in a CT image is the same as that in an X-ray image. In order to convert a CT image dataset into a 2 dimensional X-ray image, the simplest operations necessary are to first integrate the voxel values in the CT image data and subsequently to normalize the resulting 2D image.

Fluoroscopy systems (Figure 3.4) work very similar to X-ray devices in that they consist of a source and a fluorescent screen, each mounted at one of the ends of a C-shaped body (C-Arm) which can rotate to give variety of imaging angles.

The 2D image obtained through fluoroscopy has the opposite intensity mapping as that of a 2D X-ray image. One of the objectives of this project was to eliminate radiation exposure in the training environment. One design component toward accomplishing this goal was to generate an artifical fluoroscopy image of a physical joint based on a CT dataset. Given the relationships described here between 3D CT

Figure 3.4: Fluoroscopy System(C-Arm) [72].

image dataset, 2D X-ray image and 2D fluoroscopy image it is possible to create the image library of various angle fluoroscopy scans of the joint model. To convert the 3D dataset into 2D images (either x-ray type, or fluoroscopy type) the following steps were performed (as described in the following section):

- Computed tomography acquisition of the object of interest.

- Image scaling - to compensate for differences in voxel sizes between the 3D data set and the intended 2D image.

- Orientation of the data set to the appropriate viewing angles and integration through the data set.

- Post-processing to create fluoroscopy-type images with appropriate pixel intensities.

3.2.1 3D Computed Tomography Acquisition

Computed tomography images were obtained with two different machines. The synthetic femur image data was obtained using a Siemens scanner (0.25-by-0.25 mm pixel spacing at a slice thickness of 0.75 mm). The image dataset of the hip joint model was obtained using a Philips scanner (0.24-by-0.24 mm pixel spacing at a slice thickness of 1 mm). Presence of metal objects in the CT scanner generates artifacts. This is mainly due to "beam hardening" effect. Beam hardening results in non-linear absorption of X-ray beams. This phenomenon occurs because of the polychromatic nature of the CT X-ray beams. The low energy photons are absorbed as the beam passes through the object while the high energy photons are not. This process modifies the mixture of the beam through eliminating the low energy components, leading to "beam hardening". This effect is rectified in the process of acquisition and reconstruction of the images for tissue-like material. However, when a metal object is being scanned this correction is not very accurate and will lead to artifacts [73].

The mismatch in the density of metal objects compared to tissue means the flux of photons through each will be characterized differently. Therefore in a scanner that is designed for tissue, scanning of metal objects will cause incorrect calculations during reconstruction process. Furthermore, the quantum error that is present will be much higher in the metal object scan compared to projections that do not pass through such material. Therefore, in medical scans of patients who have a prosthesis it is necessary to take into account the difference in the error when processing the raw image data [74].

Philips healthcare has created a reconstruction algorithm called O-MAR (orthopedic metal artifact reduction), which as the name implies, aims to reduce the artifacts present in the medical images due to presence of metal objects such as implants. This algorithm works by separating the metal image from the tissue classified image, otherwise non-metal image. Additionally the sinogram of these images are generated and through subtraction of tissue classified sinogram from the original image sinogram the error sinogram is produced. The metal sinogram is then used as a mask to remove all the non-metal data points. Finally by backprojecting this error sinogram data, the corrected image is generated [75]. By using this algorithm to reconstruct the scans of the surgical tools as well as the hip joint model (the hip joint model also included a few stainless steel parts), it was possible to obtain a very good quality CT image dataset.

3.2.2 Pre-Processing Step-Image Scaling

CT image data are organized into slices. Each slice consists of a number of pixels depending on the accuracy of reconstruction. Unlike in Micro-CT systems where the voxels are isometric, the clinical CT scanners usually have a different in-plane pixel size than the slice thickness [71]. Therefore, it is necessary to scale the 3D image data in order to represent the object in the scan with correct geometry. Scaling was accomplished through image interpolation. Image interpolation leads to increased size of image data and requires computing power. Interpolation is often performed on digital images to evaluate the intensity values at non-discrete-valued locations [68]. A function can be defined to represent the change in the intensity

of the voxels within an image. This function can be used to estimate the intensity values at any desired location within the image. Linear interpolation is quite a simple procedure where the average of the values at the neighboring pixel locations are used to estimate a value for the non-integer pixel locations [68]. Figure 3.5 illustrates an example of bilinear interpolation. In this case the pixel of interest, $f(1.6, 1.5)$, is non-discrete in both directions. Therefore a series of linear interpolations are necessary to evaluate the pixel value. In other words, a first linear interpolation is performed between the two consecutive pixels $f(1, 1)$ and $f(1, 2)$ to obtained $f(1, 1.5)$, then a second linear interpolation is performed between $f(2, 1)$ and $f(2, 2)$ to find the pixel value at $f(2, 1.5)$. Subsequently, a third linear interpolation is performed between the resulting non-discrete pixels to obtain $f(1.6, 1.5)$. As the joint model used in this project did not include any significant details that must be carefully taken into account, a simple linear interpolation was utilized to scale the images.

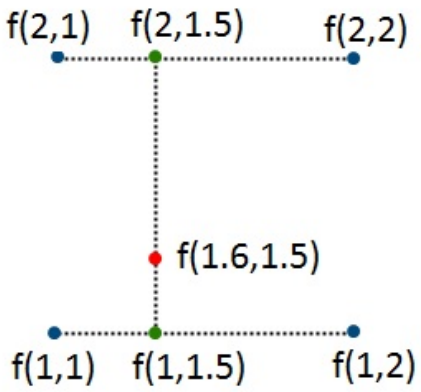

Figure 3.5: Bilinear interpolation, a sequence of linear interpolation.

3.2.3 Virtual X-ray Image Generation

Using a fluoroscopy system in the operating room, the images of the joint can be obtained at various angles. To mimic this in the virtual system the 3D CT dataset was projected along different directions to form a 2D image as though from different viewing angles. Alternatively, the 3D image data could be rotated and the projection could be performed along a fixed direction after each rotation. The latter requires more processing power. This is because when rotating the 3 dimensional image data the computer needs to handle the entire dataset altogether, whereas no such action is necessary when projecting the data at an angle. Meanwhile both of these methods create identical images. An algorithm was developed to perform projection of the CT image data at various input angles to create the 2D virtual fluoroscopy image library. This algorithm processed the 3D CT image dataset one slice at a time. Depending on the angle defined by the user a series of projection lines were defined on the image slice and all the pixels along these projection lines were integrated separately. As Figure 3.6 illustrates, the result of this operation on one image slice of the 3D dataset made up a single line of the 2D data that appeared in the final X-ray image. This process was repeated for all the image slices of the 3D CT dataset to create the complete 2D X-ray image.

3.2.4 Post-Processing-Fluoroscopy Image Generation

Once the 2D X-ray image has been created by integration of the 3D CT data, the resulting image pixels will contain values that are very close to each other. This

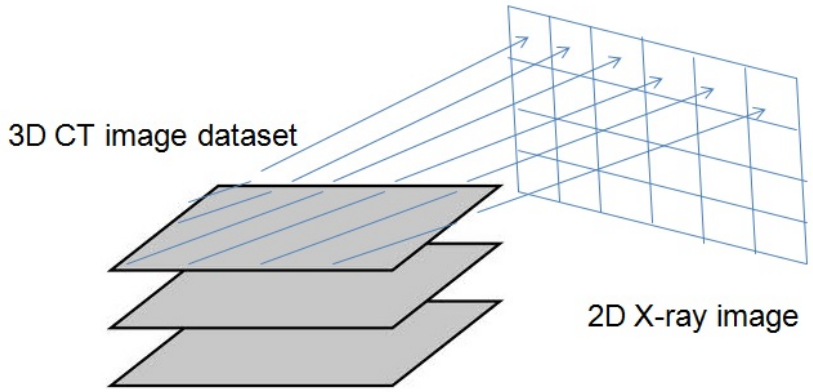

Figure 3.6: Conversion of a 3D CT image slice to a line of data in a 2D X-ray image.

is because these values are obtained by adding all the pixels along the line of integration. If this image were to be displayed the result would show a dark image in which no object could be identified. Therefore it is necessary to normalize the intensity mappings in order to obtain a realistic representation of the inhomogeneous structures in the scan. Normalization of images are performed to fit the intensity values in a set range, often 0-1 and 0-255 [68]. An algorithm was developed in MATLAB (7.10.0, The MathWorks Inc., Natick, Massachusetts) to normalize the images of the joint model to the range 0-255. The intensity values of each of the normalized X-ray images were re-mapped in order to create the virtual fluoroscopy image library. Figure 3.7 illustrates the outcome of aforementioned image processing techniques to obtain an antero-posterior (AP) fluoroscopy view of the synthetic femur.

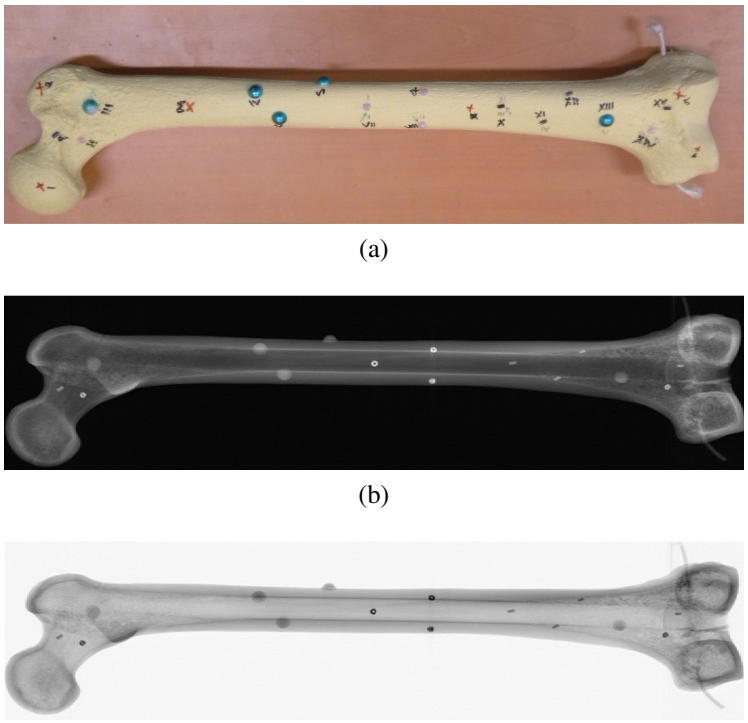

(a)

(b)

(c)

Figure 3.7: (a) Synthetic femur, and image resulting from (b) integration of CT image data, and (c) complementing the intensity map of X-ray image.

3.3 Virtual Fluoroscopy Image Formation of the Surgical Tool

In order to complete the creation of the display image in the training system, the knowledge of the spatial location of the surgical tools with respect to the joint model is necessary. This makes it possible to overlay the image of the surgical tools on top of the fluoroscopy image of the joint model. The image data of the tool was obtained using the Philips scanner (0.24-by-0.24 mm pixel spacing at a slice thickness of 1 mm). The surgical tools as well as the tool holder are usually made up of stainless

steel. Therefore the reconstruction of the image data was performed using the O-MAR algorithm. In the case of the fluoroscopy image of the surgical tool there is no need to create the virtual images at different views. This is because the surgical tools are cylindrical shaped objects and the X-ray image obtained of any of them would look like a long rectangle. Therefore, only one orthogonal view of the virtual fluoroscopy image of the tools was created.

The process of modifying the 3D CT image data to obtain the 2D virtual fluoroscopy image was identical to that for the hip joint model, as described in the previous section. As the voxels were not isometric in the Philips CT scanner, it was necessary to utilize interpolation to turn the original image dataset into a geometrically correct image data. The projection of the tool was obtained through integrating the pixel values in a direction orthogonal to the long axis of the tool. The resulting 2D X-ray projection was normalized to the range 0-255. Finally, intensity mapping was performed on this normalized X-ray image to obtained the complemented image (ie. the virtual fluoroscopy image of the tool).

3.4 Tracking

To determine the position and orientation of the surgical tools relative to the physical joint model, it was necessary to incorporate a tracking system to track the tools in three dimensional space. In this project two tracking systems were explored; firstly a mechanical tracking system (Phantom, SensAble Technologies Inc.) was used for the initial stages of development of the system. Though very accurate,

the mechanical tracking system has some limitations for practical use including restricted motion and high cost. With the aim of improving freedom of motion for the trainee and reducing cost of the system an electromagnetic tracking system (Patriot, Polhemus) was also tested.

3.4.1 Mechanical Tracker

For the proof-of-concept stage of the project a mechanical tracking system (Phantom, SensAble Technologies) was utilized to take advantage of its reliable performance and precision. The mechanical arm (Figure 3.8) consist of two links connected to a base. The links are joined together through revolute joints and therefore can move with respect to each other in single axis rotation while the base rotates about its vertical axis. This creates three variable angles, q_1, the angle of rotation of base, q_2, the angle between base and first link, and q_3, the angle between the first and the second link. Furthermore, a unique coordinate frame is associated with each joint to simplify the definition of a relation between that joint and the frame associated with the base of the mechanical tracking system.

The knowledge of the three variable angles, together with the length of the links, makes it possible to track the tip of the last link (henceforth called the "end-effector"). This system outputs a matrix that relates any point in the end-effector's coordinate frame to the coordinate frame of the base. The parameters that describe this relationship are the translation and rotation parameters and they are often represented

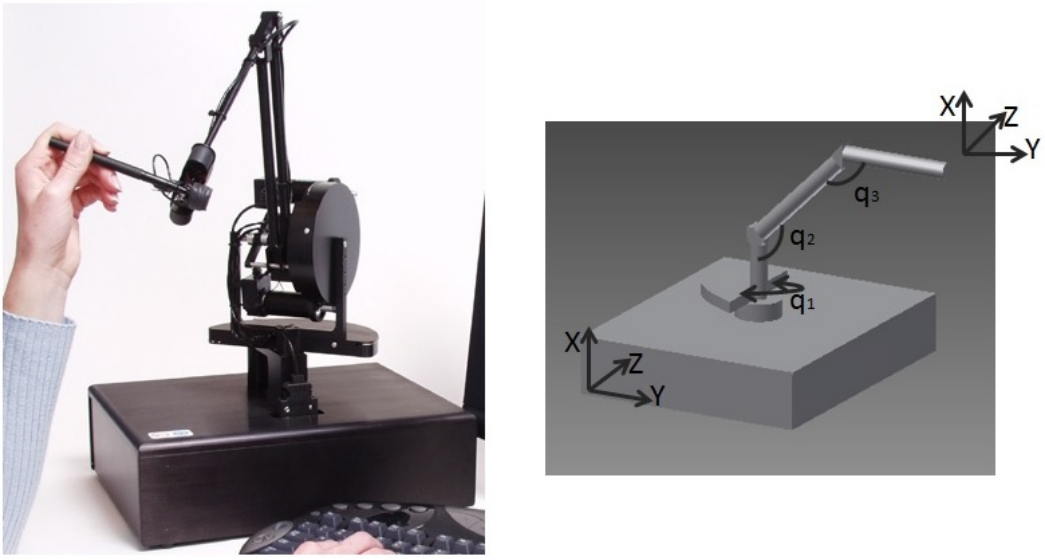

Figure 3.8: The mechanical arm[76].

in a 4-by-4 matrix in the following format [49]:

$$M_B^A = \begin{bmatrix} R_{11} & R_{12} & R_{13} & T_x \\ R_{21} & R_{22} & R_{23} & T_y \\ R_{31} & R_{32} & R_{33} & T_z \\ 0 & 0 & 0 & 1 \end{bmatrix} \tag{3.1}$$

In the above matrix, M_B^A is the transformation matrix that converts frame A into frame B. R_{ij} is the representation of a projection of the axis i of the coordinate system A into the axis j of the coordinate system B. T_k terms represent the translation along the direction k.

Registration of the physical joint model to its 3 dimensional CT image dataset is

also performed by defining a set of transformation and rotation parameters. Whereas the definition of these parameters is possible through the joint variables for the tracking system, they must be solved for in the case of registration of physical to image coordinate frame. Registration can be performed by using either fiducial markers or physiological landmarks [62, 77, 78]. The coordinates of these markers are known in the image frame and the tracking system can define their corresponding coordinates in its own frame. The transformation of the coordinates of the tip of the tool into the CT image coordinate system can be obtained by multiplying the corresponding intermediate transformations in the correct order. This relationship is described in Equation 3.2, where T_Y^X is the transformation from coordinate frame X to coordinate frame Y.

$$T_{End}^{Tool}.T_{Arm}^{End}.T_{CT}^{Arm} = T_{CT}^{Tool} \tag{3.2}$$

In Equation 3.2, T_{End}^{Tool} and T_{CT}^{Arm} terms are unknown. Using a known set of coordinates in the coordinate frames of the CT and the tracker a system of equations can be set up to solve for these transformation parameters. If P_i represents a point in the image coordinate frame and P_{TS} is the corresponding point in the tracker's coordinate frame, the two points are related to each other through Equation 3.3. Solving this system of equations requires four sets of points (12 unknown transformation parameters and 3 equations can be obtained from each point; $\frac{12}{3} = 4$).

$$T_{End}^{Tool}.T_{Arm}^{End}.T_{CT}^{Arm}.P_{TS} = P_i \tag{3.3}$$

Another solution that better represents the system can be obtained by using more than 4 sets of points to create an overdetermined system of equations. In this stage of the project 15 fiducial markers were placed on a synthetic femur model(Figure 3.7), however only 13 of these markers were in the range of reach of the mechanical tracker. Using this method the parameters were found through solving an optimization problem with the following cost function:

$$C = \sum_{k=1}^{N} ||T_{End}^{Tool}.T_{Arm}^{End}.T_{CT}^{Arm}.P_{TS}^{k} - P_{i}^{k}||^2 \tag{3.4}$$

where N = 13. The unknowns in this system of nonlinear equations were optimized using an algorithm described previously [79]. Once the parameters were defined the three transformations, T_{End}^{Tool}, T_{Arm}^{End}, and T_{CT}^{Arm} were multiplied to obtain T_{CT}^{Tool}. Using this transformation any point at the tip of the tool could be translated to its corresponding coordinates in the CT image coordinate.

3.4.2 Electromagnetic Tracker

The physical constraints of mechanical tracking system was quite evident throughout the initial development of this project. While the accuracy of mechanical tracking makes such systems ideal for the type of application where high precision is desired, the limited range of free motion that they offer makes them less popular [47]. Particularly for this application, it is necessary that the trainee be able to move freely in the field in order to achieve a correct and comfortable orientation for the surgical tools. Therefore, a less constrained tracking system was explored in the

next stage of the project. The Polhemus Patriot (Polhemus, Colchester, VT) is an electromagnetic tracking system with sensors and a field generator that are wired to the main processing unit. The sensors were relatively small (0.900 inches-by-1.113 inches-by-0.600 inches), however they were large enough that it was not possible to position them at or near the tip of the tool. Therefore, the sensors were positioned on the tool holder and at a known orientation with respect to the tip of the tool. The tracking system returned a set of position and orientation parameters for the sensor with respect to the base coordinate frame, which in turn was defined by the field generator. Each sensor had a coordinate frame (henceforth referred to as sensor frame) that was associated with it and was described by these position and orientation parameters. Figure 3.9 illustrates an example of a relationship between a sensor frame and the base frame. In this particular orientation, the information about the orientation of the sensor is obtained by noting that it is firstly rotated at an angle ψ about the Z-axis, then at an angle -θ about the new Y-axis, and finally at an angle ϕ about the X-axis. In other words, Figure 3.9 illustrates a positive azimuth angle, a negative elevation angle and a positive roll angle. Using the rotation parameters of the sensor and its position it was possible to determine the position of the tip of the tool that the sensor was sitting on. Similar to the setup of equations in the case of the mechanical tracker, an overdetermined system of equations was set up to solve for the unknowns of Equation 3.5.

$$T^{Tool}_{Sensor}.T^{Sensor}_{Base}.T^{Base}_{CT} = T^{Tool}_{CT} \tag{3.5}$$

(a)

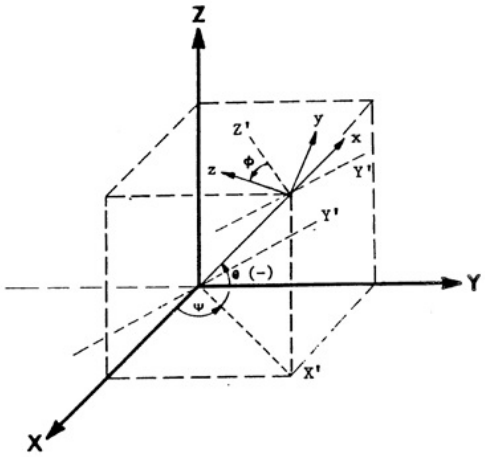

(b)

Figure 3.9: (a) Polhemus Patriot tracking system, (b) Relationship between coordinate frames(Polhemus Patriot User Manual).

The primary approach in defining T_{Sensor}^{Tool} in Equation 3.5 was to first construct the transformation matrix, defined by the Euler angles, that described the orientation of the sensor with respect to the base frame. In this case the translation parameters were described in the vector describing the position of the sensor in the base frame, whereas the rotation parameters were obtained using the angles that described the sensor's orientation with respect to the base frame. These transformation parameters were then put in a matrix similar to that described in (3.1). For the Polhemus Patriot the orientation of the sensor was described by first identifying the rotation

of X and Y reference axes about the Z-axis (the angle ψ or azimuth), subsequently defining the rotation of the Z reference axis and the new X reference axis (resulting from the first rotation) about the new Y reference axis (the angle θ or elevation), and finally the rotation of the new Y and Z reference axes with respect to the X-axis of the sensor (the angle ϕ or roll). In other words if $R_Z(\psi)$ denotes the first rotation described above, $R_Y(\theta)$ describes the second rotation, and $R_X(\phi)$ describes the third rotation, then the rotation matrix describing the orientation of the sensor in the base frame is obtained through the sequence of multiplication described in Equation 3.6 (Yaw-Pitch-Roll).

$$R_{Sensor}^{Base} = R_Z(\psi).R_Y(\theta).R_X(\phi) \tag{3.6}$$

Equations 3.7-3.9 show the representation of each of these rotation matrices as functions of the angles of rotation. While this method of defining the orientation of sensor is easy and straight forward, it is a vulnerable technique, as at certain orientations where two of the axes are aligned the phenomenon of gimbal lock can prevent the calculation of a valid orientation information.

$$R_X(\phi) = \begin{bmatrix} 1 & 0 & 0 \\ 0 & cos(\phi) & -sin(\phi) \\ 0 & sin(\phi) & cos(\phi) \end{bmatrix} \tag{3.7}$$

$$R_Y(\theta) = \begin{bmatrix} cos(\theta) & 0 & sin(\theta) \\ 0 & 1 & 0 \\ -sin(\theta) & 0 & cos(\theta) \end{bmatrix} \tag{3.8}$$

$$R_Z(\psi) = \begin{bmatrix} cos(\psi) & -sin(\psi) & 0 \\ sin(\psi & cos(\psi) & 0 \\ 0 & 0 & 1 \end{bmatrix} \tag{3.9}$$

To avoid this issue quaternions were used to define the rotation of the sensor. The matrix presented in (3.10) illustrates the definition of rotation using the four quaternion parameters, which were obtained directly from the Polhemus tracker. In this matrix q_i are the four parameters representing the vector and scalar that describe the angle-axis orientation of the sensor with respect to the base frame. q_0 is the scalar and q_1, q_2, and q_3 are the X, Y, and Z components of the vector, respectively. The translation parameters are described as the vector describing the position of the sensor in the base frame, similar to the Euler angles approach.

$$Qtrn = \begin{bmatrix} q_0^2 + q_1^2 - q_2^2 - q_3^2 & 2(q_1q_2 - q_0q_3) & 2(q_1q_3 + q_0q_2) \\ 2(q_3q_0 + q_1q_2) & q_0^2 - q_1^2 + q_2^2 - q_3^2 & 2(q_2q_3 - q_0q_1) \\ 2(q_1q_3 - q_0q_2) & 2(q_1q_0 + q_3q_2) & q_0^2 - q_1^2 - q_2^2 + q_3^2 \end{bmatrix} \tag{3.10}$$

The equations relating the two coordinate systems and the cost function are defined in a similar fashion (Equations 3.11 and 3.12).

In this stage a complete hip joint model (Figure 3.2) was used and instead of fiducial markers a total of 6 landmarks were identified in the CT and tracker coordinate frames to perform the registration.

$$T_{Sensor}^{Tool}.T_{Base}^{Sensor}.T_{CT}^{Base}.P_{TS} = P_i \tag{3.11}$$

$$C = \sum_{k=1}^{N} ||T_{Sensor}^{Tool}.T_{Base}^{Sensor}.T_{CT}^{Base}.P_{TS}^{k} - P_i^k||^2 \tag{3.12}$$

In this case N = 6. Similar algorithm as that used in the case of the mechanical arm was constructed in order to find the solution to this system of nonlinear equations [79].

In the case of the electromagnetic tracking system, it was not possible to position the sensor at the tip of the tool and therefore direct tracking of the tip could not be performed. A downside of positioning the sensor away from the tip of the tool was that the error that already existed in the readings of the tracking system would translate to a greater error in the detection of the tip (see Chapter 2, Equation 2.1). This is because an extra translation had to be performed to obtain the coordinates of the tip and the error in constructing this translation added to the existing inaccuracies of the system.

3.5 Image Overlay

Stage three of the development for this project was bringing together the separate components to function as a single and continuous system. The physical joint model

was registered to the previously obtained CT image dataset using the tracking system. Once the relationship between the two coordinate frames were known (the transformation parameters) it was possible to obtain the coordinates of the tip of the tool in the tracker coordinate frame and convert them into their corresponding coordinates in the CT image frame. This information was needed in order to perform the final 2 dimensional registration between the image of the surgical tool and that of the joint model.

In order to register two images, similar features between the two must be detected. These similar features can be the same features that appear in different parts of each image; for example if the first image is a slight variation of the same scene as in the second image (i.e. two pictures of a landscape in different seasons). On the other hand the similar features could be the 3 dimensional coordinates in space that correspond to the same point on both images; for example if the two images contain two different objects that are in the same scene at different times. The latter describes the application at hand for this project. One image contained the fluoroscopy image of the joint and the other contained the fluoroscopy image of the tool. At the time of the practice surgery, the joint and the surgical tool are both present in the work space. However, each have its own fluoroscopy image. Using the tracking system the similar features or coordinates can be detected and registration of the two images can be performed. At least two points on the surgical tool were required to perform a 2 dimensional registration of the tool and joint model fluoroscopy images; this is if the registration only requires scaling, rotation, and translation of the images used. The number of points required for registration increases if sheering

or other more complex operations are necessary in the process of registration [68]. In this project the registration was assumed to be rigid because neither the surgical tools, nor the physical joint deformed during the process. Therefore, two points were used to co-register the images. One of these points was chosen to be the tip of the tool and the other was the coordinates of the sensor on the tool holder. The coordinates of these two points were detected using the tracking systems. An algorithm was developed to overlay the projection of the orientation of the surgical tool onto the fluoroscopy images.

3.5.1 Image Overlay Algorithm-Pilot Project

In the proof-of-concept stage of the project the mechanical tracking system was used to ensure the registration is performed as accurately as possible. An algorithm is created to perform the overlaying of the surgical tool's image on the image of the joint model. The first step in the algorithm was to define two points in the coordinate frame of the physical joint; one point corresponding to the tip of the tool and another to an arbitrary point along the length of the tool. These 3D coordinates were then translated into 2D frame of the fluoroscopy images. The key step of this algorithm was the definition of an equation for the line passing through these two points in the plane of the fluoroscopy image (ie. in 2D). This line represented the projection of the tool in the fluoroscopy image of the joint model. The algorithm then re-wrote the image pixel values along this line to create a representation of the tool in the virtual fluoroscopy image of the joint. This algorithm created a single image of the joint with the projection line of the surgical tool represented as a dashed

line. The output of this algorithm is presented in Figure 3.10. This output is not

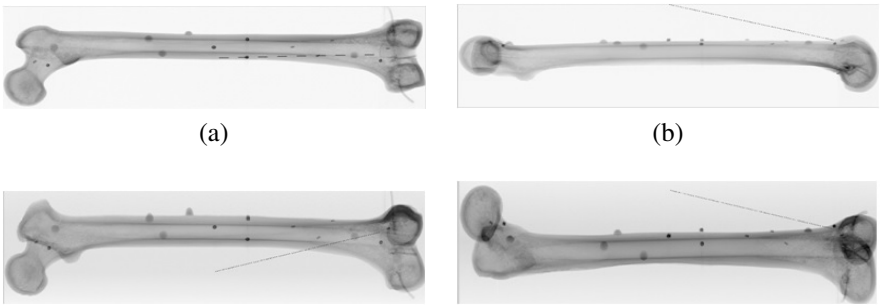

Figure 3.10: Representation of surgical tool's projection in the fluoroscopy image of the synthetic femur for (a) 0- , (b) 90-, (c) 45-, and (d)135-degree views.

a complete representation of a fluoroscopy image obtained in an operating room. While the projection of the tool provides valuable information about its orientation and position within the joint, it does not provide any geometrical information about the surgical tool. Nonetheless, for the initial development of this project the goal was to illustrate the possibility to detect and represent the orientation of the surgical tools on the fluoroscopy images of the joint. As it is illustrated by Figure 3.10 it was proven that the performance of practice surgery with simultaneous tracking of the surgical tools made the generation of virtual fluoroscopy images possible. This proof of concept was the foundation for the next stage, which included utilizing a tracking system that allows for more free motion in the work space. Also it was desired to use the CT images of the surgical tools to represent their correct geometrical shape and size.

3.5.2 Image Overlay Algorithm-Final Project

By placing the electromagnetic sensor on the surgical toolholder it was possible to detect the orientation of the tool in space. It was therefore possible to obtain as many points as desired along the line of the surgical tool. Similar to the case of the mechanical arm two points were identified to assist in overlaying of the virtual fluoroscopy image of the surgical tool on the virtual fluoroscopy image of the joint model. One point was taken as the point of contact of the sensor on the toolholder and another point was the tip of the tool, which was obtained using Equation 3.13. Here P_S is the position vector of the sensor in the base frame, P_{tip} is the position vector of the tip of the tool in the base frame, and T^{Tool}_{Sensor} is the matrix describing the transformation from sensor to the tip of the tool and its definition is described in Section 3.4.2.

$$T^{Tool}_{Sensor}.P_S = P_{tip} \tag{3.13}$$

The fluoroscopy images of the joint and the tool were co-registered. In this stage of development, instead of creating a projection line representing the orientation of the tool in the joint fluoroscopy image, the image of the tool was transformed to the correct orientation and subsequently it was overlaid on the image of the joint. The overlay algorithm aligned the fluoroscopy image of the surgical tool on top of the fluoroscopy image of the joint. By controlling the transparency of each image, simultaneous display of the two images was accomplished. An output of this algorithm is illustrated in Figure 3.11 for antero-posterior and lateral views of the joint model.

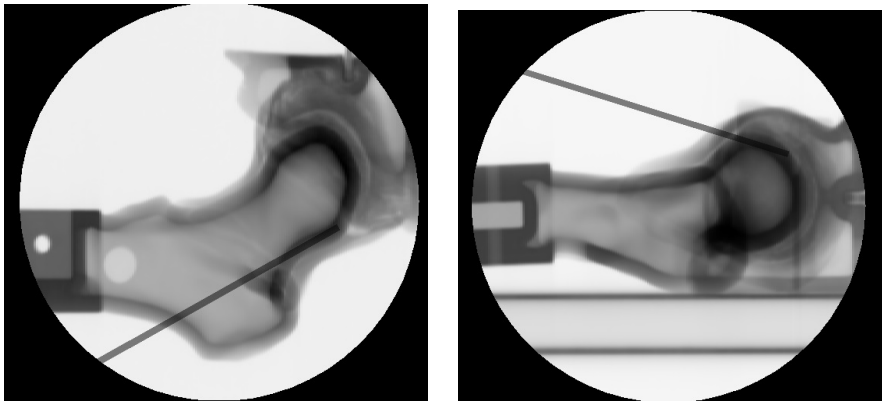

(a) (b)

Figure 3.11: Representation of surgical tool in the fluoroscopy image of the joint model in (a) antero-posterior view, (b) lateral view.

Real fluoroscopy images that are displayed for surgical staff in an operating room have a circular zone, inside of which defines the field of view of the fluoroscopy system. In order to create a similar image to that seen in an operating room, a circular mask was created and overlaid on top of the two fluoroscopy images. While the dash-line representation of the projection of tool (Figure 3.10) creates a single image, this algorithm creates a series of three images (the virtual image of the joint, the virtual image of the surgical tool, and the circular mask) overlaid on top of one another. The latter approach was found to have a better performance as the output image was produced in a shorter time. However, it is noteworthy that both algorithm had very short runtime.

CHAPTER 4

System Performance

The detail on the setup of the virtual training system was presented in the previous chapter. In this chapter, I provide the results of evaluation for the system and identify the potential future improvements. In Section 4.1 the methodology used to measure accuracy and reliability in the training system and the resulting performance of the registration algorithm for both the mechanical and electromagnetic trackers are presented. The speculations on the speed of the system and computation requirements as well as the quality of the images displayed are provided in Section 4.2. Finally, Section 4.3 presents a discussion on the outcome of the experimental analysis for the system performance.

The images used in this project were obtained in two stages. The first image dataset was obtained of a synthetic femur (Sawbones, Pacific Research Laboratories Inc., Figure 3.3 in Chapter 3), which was used for the pilot data. The synthetic femur was imaged by a Siemens scanner, 0.25-by-0.25 mm pixel spacing at a slice thickness of 0.75 mm, at St. Joseph's Hospital, Hamilton, Ontario. The second image dataset was obtained of the complete joint model (DePuy Synthes Mitek Medicine Inc., Figure 3.2 in Chapter 3) and was used in the final stage of the project. The joint model was imaged by a Philips scanner, 0.24-by-0.24 mm pixel spacing at a

slice thickness of 1 mm, at Juravinski Cancer Centre, Hamilton, Ontario. All the work in this project was performed with these image datasets.

4.1 Registration Performance

A common method in evaluating performance and accuracy in image guided surgery systems is to quantify the errors associated with registration [80, 81]. Three measures of registration accuracy have been suggested [82, 83]. Fiducial localization error (FLE) is the amount of deviation from the actual position of the fiducial to the position that is used when localization is performed. Fiducial registration error (FRE) is the root mean square of the fiducial position in the two different frames after registration. Target registration error (TRE) is the difference between the corresponding coordinates of a point, other than that used in registration, in the different coordinate frames [84, 85]. These registration errors are illustrated in Figure 4.1.

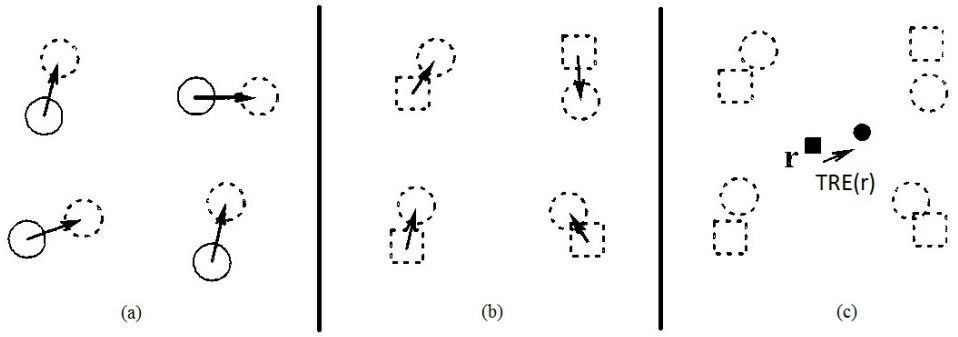

Figure 4.1: (a) Fiducial localization error, (b) fiducial registration error, (c) target registration error.

If the transformation of the two coordinate frames can be represented by Equa-

tion 4.1, FRE is calculated through Equation 4.2. Here, X_i is the coordinates of the i^{th} fiducial in one coordinate frame and $X_i^{'}$ is the coordinates of the i^{th} fiducial in the second coordinate frame, and R and T are the rotation matrix and the translation vector, respectively.

$$X_i^{'} = R.X_i + T \tag{4.1}$$

$$FRE_i = X_i^{'} - X_i \tag{4.2}$$

The study of the performance of a system often takes into account multiple control points. Therefore the error quantities (FRE and TRE) are often expressed in root mean square (RMS) format, as is shown in Equation 4.3. In this equation, M is the transformation used in registration of the two coordinate frames.

$$FRE_{RMS} = \sqrt{\frac{1}{N}\sum_{k=1}^{N} \|\overrightarrow{X_k^{'}} - M.\overrightarrow{X_k}\|^2} \tag{4.3}$$

While FRE has been most often used to reflect on the performance of such systems as those used in image guided procedures, it merely provides information on the geometric alignment of the landmarks or fiducial markers used for the process of registration (ie. it is only a testament of the validity of the transformation that describes the relationship between the two coordinate frames without considering any other impacting factors) [81]. However, the transformation parameters are not the only factors affecting the accuracy of the system. Other events such as the type and layout of fiducial markers, as well as the way they are localized also play significant role in the accuracy and reliability of the overall procedure. These factors are

solely controlled by the individual performing the procedure and not by the system. Therefore, it is recommended that newer developments make use of TRE in order to make more valid conclusions regarding performance and accuracy [80].

In order to quantify the performance of this training system the resulting RMS TRE between the physical joint model space and the final displayed image is reported. For calculation of RMS TRE, two sets of data points were identified on the synthetic femur; P_{image}, which corresponds to the coordinates of the point in the virtual fluoroscopy image, and $P_{physical}$, which corresponds to the coordinates of the point in the physical coordinate frame translated into the virtual image frame. TRE is defined as follows:

$$TRE = P^i_{image} - P^i_{physical} \tag{4.4}$$

where the superscript i identifies the i^{th} pair of homologous points. The RMS value of TRE can then be computed using the same formula as that shown in Equation 4.3.

4.1.1 Mechanical Tracking Registration Accuracy

The CT image dataset of the synthetic femur was obtained and processed in order to create the two dimensional virtual image library. The three dimensional CT images were processed using SPIN (Signal Processing In NMR, Detroit, MI) and MATLAB (7.10.0, The MathWorks Inc., Natick, Massachusetts). The image library was setup by creating fluoroscopy projections at 30-degrees increments. Furthermore, the library files were stored in the form of Mat-files, in order to preserve the dimensions of each image and make future image processing more feasible.

For this stage of testing, the tracking of the surgical tool was performed by means of a mechanical tracking system. The tool was represented by the last link of the mechanical tracker. This representation helped in avoiding the need to construct a tool holder that would be attachable to the links of the mechanical system. Attachment of a surgical tool to the mechanical arm would make the already constrained motion of the tracker more challenging. However, if a surgical tool were to be attached to the last link of the arm at a known angle, using its length from the attachment point it would have been quite possible to calculate the position of the tip of the tool. The setup of this stage is illustrated in Figure 4.2.

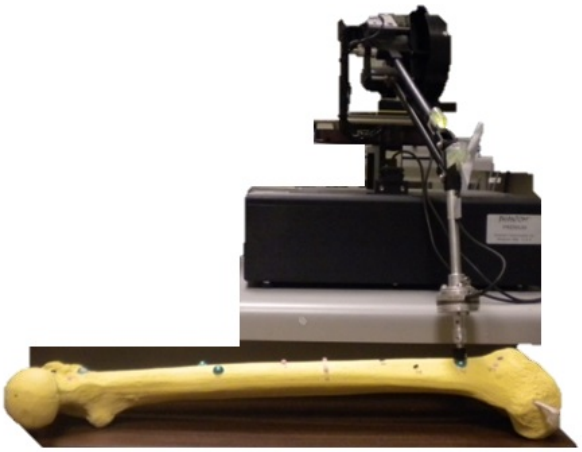

Figure 4.2: Experimental setup for the pilot stage.

Thirteen fiducial markers were in the range of reach of the mechanical arm. Four-point registration was performed in order to utilize the remaining nine markers for quantification of TRE. The X-, Y-, and Z-coordinates of each fiducial marker were identified on the CT images. In order to ensure the most accurate image coordi-

nates were obtained for the fiducial markers two orthogonal views (lateral and AP views) of the virtual X-ray image were used. The AP view provided the X- and Z-coordinates and the lateral view provided the Y- and the Z-coordinates. It was ensured that the two Z-coordinates, which corresponded to the slice number where the center of the fiducial marker was positioned, was equivalent in both views. The corresponding physical coordinates of these markers in the frame of the mechanical tracking system was obtained by touching each marker by the end-effector of the mechanical arm. The interface between the mechanical tracking system and the computer was through an algorithm, which was already created in MATLAB Simulink (Quanser Real Time Control Toolbox, Version 2.0). The relationship between the coordinates of the end-effector and the base frame of the mechanical tracker were calculated by this algorithm. TRE was evaluated with a various number of control points. At $N = 4$ TRE was evaluated at 2.0 mm. An increase of N to 5 control points increased TRE to 2.1 mm and with $N = 6$ TRE was found to be 2.5 mm (Table 4.1).

Table 4.1: Mechanical Tracker-Error analysis

No. of Control Points	RMS TRE (mm)
4	2.0
5	2.1
6	2.5

4.1.2 Electromagnetic Tracking Registration Accuracy

The interface of the electromagnetic tracking system (EMTS) with the personal computer was made through a program developed in C++ specifically for this project using Microsoft Visual Studio 2010 Express. The Polhemus trackers include a software development kit, which was utilized to create this interfacing program.

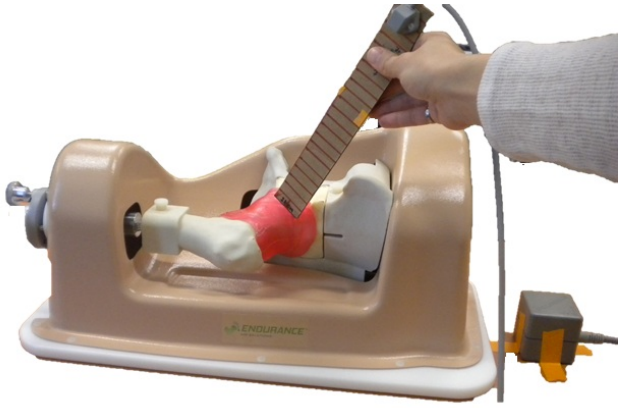

Figure 4.3: Experimental setup with the electromagnetic tracking system and hip joint model.

While the stage of the project which utilized the EMTS as the tracker included the hip joint model to represent the patient (Figure 4.3), in order to quantify target registration error for this stage of test of the system the synthetic femur was used. The reason for this was that the hip joint model was registered using anatomical landmarks that were isolated on the virtual images and the process of localizing these landmarks was error-prone. Therefore the synthetic femur model was used in order to take advantage of the fiducial markers attached to it. In the case of the EMTS, since the tracker offers a better range of motion, it was possible to utilize all 15 fiducial markers. Therefore six markers were used to perform the registration

and the remaining markers were used to evaluate target registration error.

A similar algorithm as that for mechanical tracker evaluation stage was developed in MATLAB to calculate RMS TRE for electromagnetic tracking system. For 5, 7, and 9 control points RMS TRE was calculated to be 7.6 mm, 12.4 mm, and 11.3, respectively (Table 4.2).

Table 4.2: Electromagnetic Tracker-Error analysis

No. of Control Points	RMS TRE (mm)
5	7.6
7	12.4
9	11.3

4.2 Computational Requirements

Handling three dimensional image data had a rather long processing time on the order of several hours. Furthermore the operations were performed on a personal computer with 16 GB of RAM. One of the desired characteristics of the final system was to eliminate the need to have high memory requirement for the computer component of the training system. This was the consideration that lead to the idea of creating the two dimensional virtual image library. The manipulations necessary for these two dimensional images were possible in a few seconds and therefore the speed of performance of the system was made closer to that of a fluoroscopy system. The runtime of the system was evaluated for 18 consecutive virtual fluoroscopy image displays and the average runtime of the system was found to be 2.7 seconds with standard deviation of 0.7 seconds. Moreover, using the two dimensional im-

age library made it possible to easily run the system on a personal computer with 6 GB of RAM with a 2.30 GHz processor.

Additionally, the training system did not require a particular graphics card on the computer that displays the output images. Figure 4.4 shows an example of the output of the system on the personal computer used to run the training system.

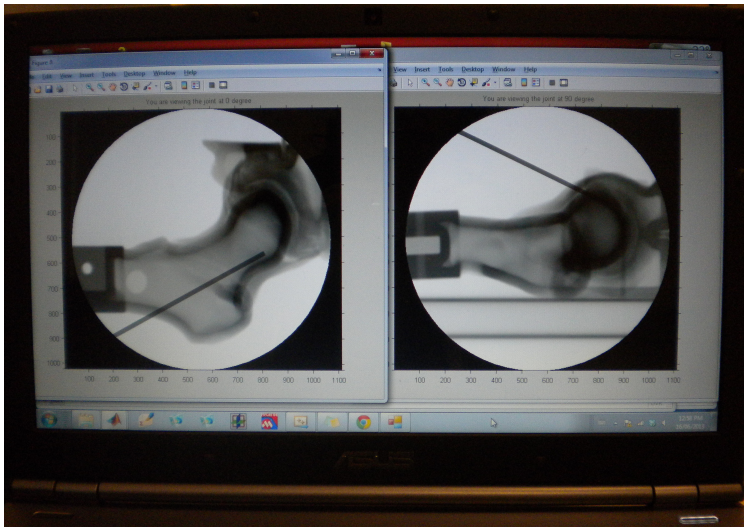

Figure 4.4: Screenshot of a virtual fluoroscopy image.

4.3 Discussion

Image guidance makes up an important part of arthroscopic surgery. In an operating room, the fluoroscopy system provides an excellent representation of the geometrical relationship between the joint and the surgical tools. Furthermore, the endoscope helps the surgeon navigate within the joint. It is therefore significant to ensure the training system is capable of providing high accuracy images that

illustrate the surgical tools within the joint space to the surgeon in training.

4.3.1 Accuracy Measures

Rigid body, point-based registration can be performed when registering non-deformable objects. Such transformations are used in performing image-guided surgery for neuro-surgery and orthopedic surgeries because the tissue in these operations is assumed to be rigid. The transformation obtained through rigid body, point-based registration is optimized through minimization of fiducial registration error. This transformation brings the coordinates of the fiducial points or the landmarks into as close as possible of an alignment [86]. The error in registration is often due to localization of these landmarks or fiducial markers (FLE) and it is quite inevitable. It has been suggested that computer assisted operations need a system accuracy of better than 1.5 mm [51, 87]. For placement of the tool in arthroscopic surgery an error of 1-2 mm is acceptable and does not lead to a significant damage to the surrounding tissue. This was set as the goal for the virtual training system performance. The identification and quantification of the accuracy of the training system was performed using FRE and TRE. FRE merely provides an estimation of the validity of the rigid body registration [80]. Nonetheless, if the FRE for one system is greater than normal, it can be expected that the registration is not a very reliable process. This could be either due to inaccurate localization of the fiducial markers while performing registration or because of potential motion of the fiducial markers leading to mismatch of their physical location compared to their position in the image slices.

It has been shown that while many surgeons traditionally considered FRE as the measure of accuracy of the system, it is in fact an unreliable indicator of accuracy of the registration [80, 86]. Target registration error has been used to quantify the accuracy of the system in localizing the targets that are not used in the registration process.

In this project the first stage of the experiments with the mechanical tracker resulted in quite an accurate performance with the TRE ranging between 2.0 mm and 2.5 mm. While the TRE was found to be outside of 1-2 mm range, it must be noted that the constraints on the motion of the mechanical tracker had a significant contribution in compromising the performance of the system at this stage. The setup of the system with the mechanical tracker was difficult to modify and access to a number of the fiducial markers were rather difficult. Therefore, it was expected that the registration process would introduce inaccuracy in the system. Taking the inconsistency in localizing the different fiducial markers into account, it can be concluded that the range of TRE obtained for this stage of the project was good.

When using the electromagnetic tracking system, the RMS TRE was found to increase. While the localization of fiducial markers as well as the targets are more easily performed using such a system that allows for a more free range of motion, the susceptibility of the electromagnetic tracking system to metal interference was found to degrade its functionality. This issue was significant to a point that surgical tools and the tool holder, which are made of stainless steel material, could not be utilized in the process of testing. Therefore, a rectangular piece of cardboard was used; the electromagnetic sensor was mounted on one end of the cardboard and a

point was identified at the other end of the rectangular piece to represent the tip of the tool. The benefit of using a rectangular piece with a known dimension was that, using such a geometry, the definition of a vector describing the tip of the tool in the coordinate frame of the sensor was made very much easier. However the structure allowed for some deformation (i.e. bending) and this contributed to the inaccuracy of the system setup in this stage. Furthermore, the deviation in the definition of the tip of the tool between each localization step was another source of error for this setup. The RMS TRE in this stage of the project was identified for 5, 7, and 9 control points and the resulting values were 7.6 mm, 12.4 mm, and 11.3, respectively, which indicates a significant level of inaccuracy. The fluctuating trend of the error which is observed with the increase in the number of control points is evidence of the random nature of error in the electromagnetic tracking system readings. Fiducial registration error was then considered in order to identify the cause of this error observed in RMS TRE. The RMS FRE for 5 fiducial markers was found to be 5.6 mm, for 10 markers it was 5.0 mm, and for 15 markers it was 9.3 mm. The increasing trend of RMS FRE can also lead to conclusion that the nature of noise in the electromagnetic tracking system is random.

From the results presented it can be concluded that the electromagnetic tracking system is not the most accurate tracking method. While it offers great range of motion and a decent range of operation for the size of the joint model used in this project, the susceptibility of the system to electromagnetic interference prevents the use of surgical tools. Meanwhile, the mechanical tracking system offers a very good tracking performance, however the high cost of a good mechanical tracker as well

as the constrained range of motion that it offers makes it less favored for application in this training system.

CHAPTER 5

Conclusion and Future Work

The primary objective of this work was to create a novel training system for training new surgeons in performing arthroscopic procedures. The proposed training system made use of tracking technologies and various image processing techniques to merge the physical work space with the virtual image library, which was previously created and stored in the system.

The challenges in the development of this system included the choice of a suitable tracking system and an efficient design of an algorithm to generate the virtual fluoroscopy images for display. Several tracking systems are available and four were considered for this project. The primary characteristics of interest for the tracking system were the range of motion that it allows and the accuracy level that it offers. A mechanical tracking system was initially tested for the proof of the concept behind this novel training system. In the next iteration an electromagnetic tracking system was used, which offered a good range of accuracy and great range of motion within the field of operation.

It was found that the image processing techniques used in this project, successfully created a system that functioned in real time and generated very good virtual fluoroscopy images. However the error analysis demonstrated that there were issues

with the target registration accuracy. The quantified error for the setup of the system with the mechanical tracker was within an acceptable range. However, this setup did not allow for full range of free motion in the field of operation. A good range of motion is desired because the training must provide an opportunity for the trainees to experiment with different ways of handling surgical tools in order to develop correct and comfortable approaches in conducting procedures. The setup of the system with the electromagnetic tracking system did not allow for testing to be performed with the surgical tools. This was because the presence of stainless steel surgical tools caused significant amount of interference in the electromagnetic field of the tracking system. This tracking system resulted in an error range beyond what is considered acceptable in arthroscopy surgeries.

Based on the results it was concluded that, while the virtual image generation algorithm was quite successful, the current version of the system requires some improvements. It is required that the tracking system used in this system be replaced with one that offers similar range of free motion as the electromagnetic tracking system, but also is not prone to interference. In particular, the presence of actual surgical tools is a significant feature of this training system and therefore the tracking system used must allow for their utilization in the practice surgery. From consideration of four different tracking systems (mechanical, electromagnetic, ultrasonic and optical) it was concluded that optical tracking system might be the best option for this system and therefore the next tracking technology that should be tested. The ultrasonic tracking systems have been shown to have susceptibility to interference due to temperature changes. Also, presence of other objects be-

tween the transducer and the detector can cause error in the system. These aspects, make ultrasonic trackers a poorer choice compared to optical systems. However, the higher cost of optical tracking systems must be taken into consideration when making the choice between this mode of tracking and ultrasonic trackers.
In summary, according to the present state of this project, the following future steps are identified:

- Identification and testing of a new tracking system.
- Implementing a virtual tissue removal algorithm.
- Creation of a complete library of images (shoulder joint, knee joint, etc.).
- Merging of the complete system into one package.

Meanwhile, through the accomplishments of this work, a complete and working algorithm for real-time creation and handling of virtual fluoroscopy images have been developed. Furthermore, an algorithm for incorporation of a tracker into this training system has been created, which given an accurate tracking technology can complete the design of this novel system for arthroscopic surgery training.

Bibliography

[1] A. G. Gallagher, E. M. Ritter, A. B. Lederman, D. A. McClusky III, and C. D. Smith, "Video-assisted surgery represents more than a loss of three-dimensional vision," *The American journal of surgery*, vol. 189, no. 1, pp. 76–80, 2005. (Cited on page 1.)

[2] S. Azegami, D. Kosuge, and M. Ramachandran, "Surgical treatment of femoroacetabular impingement in patients with slipped capital femoral epiphysis a review of current surgical techniques," *Bone & Joint Journal*, vol. 95, no. 4, pp. 445–451, 2013. (Cited on pages 1 and 13.)

[3] C. Diaz-Ledezma and J. Parvizi, "Surgical approaches for cam femoroacetabular impingement: The use of multicriteria decision analysis," *Clinical Orthopaedics and Related Research®*, pp. 1–8, 2013. (Cited on page 2.)

[4] M. J. Philippon, M. L. Schenker, K. K. Briggs, D. A. Kuppersmith, R. B. Maxwell, and A. J. Stubbs, "Revision hip arthroscopy," *The American journal of sports medicine*, vol. 35, no. 11, pp. 1918–1921, 2007. (Cited on page 2.)

[5] Y. Benali and B. D. Katthagen, "Hip subluxation as a complication of arthroscopic debridement," *Arthroscopy: The Journal of Arthroscopic & Related Surgery*, vol. 25, no. 4, pp. 405–407, 2009. (Cited on page 2.)

[6] D. K. Matsuda, "Acute iatrogenic dislocation following hip impingement arthroscopic surgery," *Arthroscopy: The Journal of Arthroscopic & Related Surgery*, vol. 25, no. 4, pp. 400–404, 2009. (Cited on page 2.)

[7] V. M. Ilizaliturri Jr *et al.*, "Complications of arthroscopic femoroacetabular impingement treatment: a review," *Clinical orthopaedics and related research*, vol. 467, no. 3, pp. 760–768, 2009. (Cited on pages 3 and 17.)

[8] P. van der Zwaal, B. J. Thomassen, M. J. Nieuwenhuijse, R. Lindenburg, J.-W. A. Swen, and E. R. van Arkel, "Clinical outcome in all-arthroscopic versus mini-open rotator cuff repair in small to medium-sized tears: A randomized controlled trial in 100 patients with 1-year follow-up," *Arthroscopy: The Journal of Arthroscopic & Related Surgery*, 2012. (Cited on page 4.)

[9] A. H. Gomoll, R. V. OŠToole, J. Czarnecki, and J. J. Warner, "Surgical experience correlates with performance on a virtual reality simulator for shoulder arthroscopy," *The American Journal of Sports Medicine*, vol. 35, no. 6, pp. 883–888, 2007. (Cited on pages 4 and 17.)

[10] S. Srivastava, P. L. Youngblood, C. Rawn, S. Hariri, W. Heinrichs, and A. L. Ladd, "Initial evaluation of a shoulder arthroscopy simulator: establishing construct validity," *Journal of shoulder and elbow surgery*, vol. 13, no. 2, pp. 196–205, 2004. (Cited on pages 4, 17 and 19.)

[11] M. Bridges and D. L. Diamond, "The financial impact of teaching surgical residents in the operating room," *The American Journal of Surgery*, vol. 177, no. 1, pp. 28–32, 1999. (Cited on pages 4 and 6.)

[12] J. L. Irani, M. M. Mello, S. W. Ashley, E. E. Whang, M. J. Zinner, E. Breen, *et al.*, "Surgical residents' perceptions of the effects of the acgme duty hour requirements 1 year after implementation.," *Surgery*, vol. 138, no. 2, p. 246, 2005. (Cited on page 4.)

[13] J. D. Zuckerman, E. N. Kubiak, I. Immerman, and P. DiCesare, "The early effects of code 405 work rules on attitudes of orthopaedic residents and attending surgeons," *The Journal of Bone & Joint Surgery*, vol. 87, no. 4, pp. 903–908, 2005. (Cited on page 4.)

[14] K. D. Martin, P. J. Belmont, A. J. Schoenfeld, M. Todd, K. L. Cameron, and B. D. Owens, "Arthroscopic basic task performance in shoulder simulator model correlates with similar task performance in cadavers," *The Journal of Bone & Joint Surgery*, vol. 93, no. 21, pp. e127–1, 2011. (Cited on pages 5, 17 and 18.)

[15] N. E. Seymour, A. G. Gallagher, S. A. Roman, M. K. OŠBrien, V. K. Bansal, D. K. Andersen, and R. M. Satava, "Virtual reality training improves operating room performance: results of a randomized, double-blinded study," *Annals of surgery*, vol. 236, no. 4, p. 458, 2002. (Cited on pages 9, 17, 18 and 19.)

[16] R. A. Pedowitz, J. Esch, S. Snyder, *et al.*, "Evaluation of a virtual reality simulator for arthroscopy skills development," *ARTHROSCOPY-NEW YORK-*, vol. 18, no. 6, pp. E29–E29, 2002. (Cited on pages 9, 17 and 18.)

[17] R. M. Satava, "Virtual reality surgical simulator," *Surgical endoscopy*, vol. 7, no. 3, pp. 203–205, 1993. (Cited on pages 9, 18 and 19.)

[18] G. Porcellini, G. Merolla, F. Campi, A. Pellegrini, C. S. Bodanki, and P. Paladini, "Arthroscopic treatment of early glenohumeral arthritis," *Journal of Orthopaedics and Traumatology*, pp. 1–7, 2013. (Cited on page 10.)

[19] J. C. Clohisy and L. C. St John, "Surgical treatment of femoroacetabular impingement: a systematic review of the literature," *Clinical Orthopaedics and Related Research®*, vol. 468, no. 2, pp. 555–564, 2010. (Cited on page 13.)

[20] L. A. Anderson, C. L. Peters, B. B. Park, G. J. Stoddard, J. A. Erickson, and J. R. Crim, "Acetabular cartilage delamination in femoroacetabular impingementrisk factors and magnetic resonance imaging diagnosis," *The Journal of Bone & Joint Surgery*, vol. 91, no. 2, pp. 305–313, 2009. (Cited on page 13.)

[21] M. Beck, M. Leunig, J. Parvizi, V. Boutier, D. Wyss, and R. Ganz, "Anterior femoroacetabular impingement: part ii. midterm results of surgical treatment," *Clinical orthopaedics and related research*, vol. 418, pp. 67–73, 2004. (Cited on page 13.)

[22] R. Ganz, J. Parvizi, M. Beck, M. Leunig, H. Nötzli, and K. A. Siebenrock, "Femoroacetabular impingement: a cause for osteoarthritis of the hip," *Clin-*

ical orthopaedics and related research, vol. 417, pp. 112–120, 2003. (Cited on page 13.)

[23] J. Thomas Byrd, "Hip arthroscopy utilizing the supine position," *Arthroscopy: The Journal of Arthroscopic & Related Surgery*, vol. 10, no. 3, pp. 275–280, 1994. (Cited on page 13.)

[24] H. Nötzli, T. Wyss, C. Stoecklin, M. Schmid, K. Treiber, and J. Hodler, "The contour of the femoral head-neck junction as a predictor for the risk of anterior impingement," *Journal of Bone & Joint Surgery, British Volume*, vol. 84, no. 4, pp. 556–560, 2002. (Cited on page 13.)

[25] M. Leunig, M. M. Casillas, M. Hamlet, O. Hersche, H. Nötzli, T. Slongo, and R. Ganz, "Slipped capital femoral epiphysis: early mechanical damage to the acetabular cartilage by a prominent femoral metaphysis," *Acta Orthopaedica*, vol. 71, no. 4, pp. 370–375, 2000. (Cited on page 14.)

[26] J. Parvizi, M. Leunig, and R. Ganz, "Femoroacetabular impingement," *Journal of the American Academy of Orthopaedic Surgeons*, vol. 15, no. 9, pp. 561–570, 2007. (Cited on page 14.)

[27] M. Lavigne, J. Parvizi, M. Beck, K. A. Siebenrock, R. Ganz, and M. Leunig, "Anterior femoroacetabular impingement: part i. techniques of joint preserving surgery," *Clinical orthopaedics and related research*, vol. 418, pp. 61–66, 2004. (Cited on page 14.)

[28] A. McCarthy, P. Harley, and R. SmallwoodI, "Virtual arthroscopy training," *Medicine Meets Virtual Reality, 8: The Convergence of Physical and Informational Technologies: Options for a New Era in Health Care*, vol. 62, p. 221, 1999. (Cited on page 17.)

[29] W. D. Cannon, D. G. Eckhoff, W. E. Garrett Jr, R. E. Hunter, and H. J. Sweeney, "Report of a group developing a virtual reality simulator for arthroscopic surgery of the knee joint," *Clinical orthopaedics and related research*, vol. 442, pp. 21–29, 2006. (Cited on page 17.)

[30] J. D. Michelson, "Simulation in orthopaedic education: an overview of theory and practice," *The Journal of Bone & Joint Surgery*, vol. 88, no. 6, pp. 1405–1411, 2006. (Cited on page 17.)

[31] A. H. Gomoll, G. Pappas, B. Forsythe, and J. J. Warner, "Individual skill progression on a virtual reality simulator for shoulder arthroscopy a 3-year follow-up study," *The American Journal of Sports Medicine*, vol. 36, no. 6, pp. 1139–1142, 2008. (Cited on page 17.)

[32] N. Howells, H. Gill, A. Carr, A. Price, and J. Rees, "Transferring simulated arthroscopic skills to the operating theatre," *Journal Of Bone And Joint Surgery-British Volume-*, vol. 90, no. 4, p. 494, 2008. (Cited on page 17.)

[33] J. A. Oostema, M. P. Abdel, and J. C. Gould, "Time-efficient laparoscopic skills assessment using an augmented-reality simulator," *Surgical endoscopy*, vol. 22, no. 12, pp. 2621–2624, 2008. (Cited on page 17.)

[34] T. P. Grantcharov, V. Kristiansen, J. Bendix, L. Bardram, J. Rosenberg, and P. Funch-Jensen, "Randomized clinical trial of virtual reality simulation for laparoscopic skills training," *British Journal of Surgery*, vol. 91, no. 2, pp. 146–150, 2004. (Cited on page 17.)

[35] D. J. Anastakis, G. Regehr, R. K. Reznick, M. Cusimano, J. Murnaghan, M. Brown, and C. Hutchison, "Assessment of technical skills transfer from the bench training model to the human model," *The American journal of surgery*, vol. 177, no. 2, pp. 167–170, 1999. (Cited on page 17.)

[36] O. Van der Meijden and M. Schijven, "The value of haptic feedback in conventional and robot-assisted minimal invasive surgery and virtual reality training: a current review," *Surgical endoscopy*, vol. 23, no. 6, pp. 1180–1190, 2009. (Cited on page 18.)

[37] K. Atesok, J. D. Mabrey, L. M. Jazrawi, and K. A. Egol, "Surgical simulation in orthopaedic skills training," *Journal of the American Academy of Orthopaedic Surgeons*, vol. 20, no. 7, pp. 410–422, 2012. (Cited on page 18.)

[38] J. Psotka, "Immersive training systems: Virtual reality and education and training," *Instructional science*, vol. 23, no. 5-6, pp. 405–431, 1995. (Cited on page 19.)

[39] M. Vankipuram, K. Kahol, A. McLaren, and S. Panchanathan, "A virtual reality simulator for orthopedic basic skills: A design and validation study,"

Journal of biomedical informatics, vol. 43, no. 5, pp. 661–668, 2010. (Cited on page 19.)

[40] R. Zajtchuk and R. M. Satava, "Medical applications of virtual reality," *Communications of the ACM*, vol. 40, no. 9, pp. 63–64, 1997. (Cited on page 19.)

[41] M. T. Schultheis and A. A. Rizzo, "The application of virtual reality technology in rehabilitation," *Rehabilitation Psychology*, vol. 46, no. 3, pp. 296–311, 2001. (Cited on page 19.)

[42] J. Vora, S. Nair, A. K. Gramopadhye, A. T. Duchowski, B. J. Melloy, and B. Kanki, "Using virtual reality technology for aircraft visual inspection training: presence and comparison studies," *Applied Ergonomics*, vol. 33, no. 6, pp. 559–570, 2002. (Cited on page 19.)

[43] R. B. Davis, S. Ounpuu, D. Tyburski, and J. R. Gage, "A gait analysis data collection and reduction technique," *Human Movement Science*, vol. 10, no. 5, pp. 575–587, 1991. (Cited on page 19.)

[44] J. K. Aggarwal and Q. Cai, "Human motion analysis: A review," in *Nonrigid and Articulated Motion Workshop, 1997. Proceedings., IEEE*, pp. 90–102, IEEE, 1997. (Cited on page 19.)

[45] M. Chmarra, C. Grimbergen, and J. Dankelman, "Systems for tracking minimally invasive surgical instruments," *Minimally Invasive Therapy & Allied Technologies*, vol. 16, no. 6, pp. 328–340, 2007. (Cited on page 20.)

[46] A. D. Wiles, D. G. Thompson, and D. D. Frantz, "Accuracy assessment and interpretation for optical tracking systems," in *Medical Imaging 2004*, pp. 421–432, International Society for Optics and Photonics, 2004. (Cited on pages 20, 23 and 30.)

[47] G. Welch and E. Foxlin, "Motion tracking: No silver bullet, but a respectable arsenal," *Computer Graphics and Applications, IEEE*, vol. 22, no. 6, pp. 24–38, 2002. (Cited on pages 21, 28, 30 and 60.)

[48] N. D. Glossop, "Advantages of optical compared with electromagnetic tracking," *The Journal of Bone & Joint Surgery*, vol. 91, no. Supplement_1, pp. 23–28, 2009. (Cited on pages 21, 22, 23, 24, 25, 26, 27, 28 and 29.)

[49] L. Sciavicco and B. Siciliano, *Modelling and control of robot manipulators*. Springer Verlag, 2000. (Cited on pages 21, 37 and 58.)

[50] C. Nafis, V. Jensen, L. Beauregard, and P. Anderson, "Method for estimating dynamic em tracking accuracy of surgical navigation tools," in *Medical Imaging*, pp. 61410K–61410K, International Society for Optics and Photonics, 2006. (Cited on page 23.)

[51] W. Birkfellner, F. Watzinger, F. Wanschitz, R. Ewers, and H. Bergmann, "Calibration of tracking systems in a surgical environment," *Medical Imaging, IEEE Transactions on*, vol. 17, no. 5, pp. 737–742, 1998. (Cited on pages 23, 32 and 80.)

[52] R. Aguilar, H. Kerkvliet, and G. Meijer, "High-resolution low-cost ultrasonic tracking system for human-interface systems," in *Instrumentation and Measurement Technology Conference, 2005. IMTC 2005. Proceedings of the IEEE*, vol. 2, pp. 878–882, IEEE, 2005. (Cited on page 25.)

[53] W. Birkfellner, F. Watzinger, F. Wanschitz, G. Enislidis, C. Kollmann, D. Rafolt, R. Nowotny, R. Ewers, and H. Bergmann, "Systematic distortions in magnetic position digitizers," *Medical physics*, vol. 25, p. 2242, 1998. (Cited on pages 26 and 28.)

[54] F. H. Raab, E. B. Blood, T. O. Steiner, and H. R. Jones, "Magnetic position and orientation tracking system," *Aerospace and Electronic Systems, IEEE Transactions on*, no. 5, pp. 709–718, 1979. (Cited on page 28.)

[55] J. Hummel, M. Figl, C. Kollmann, H. Bergmann, and W. Birkfellner, "Evaluation of a miniature electromagnetic position tracker," *Medical physics*, vol. 29, p. 2205, 2002. (Cited on pages 28 and 29.)

[56] W. M. Ricci, T. A. Russell, D. M. Kahler, L. Terrill-Grisoni, and P. Culley, "A comparison of optical and electromagnetic computer-assisted navigation systems for fluoroscopic targeting," *Journal of orthopaedic trauma*, vol. 22, no. 3, pp. 190–194, 2008. (Cited on page 29.)

[57] C. Burri. Email quote, 09-27-2012. (Cited on page 31.)

[58] R. Syed. Email quote, 07-02-2013. (Cited on page 31.)

[59] S. M. Crawford. Email quote, 09-26-2012. (Cited on page 31.)

[60] N. Schell. Email quote, 11-13-2012. (Cited on page 31.)

[61] M. Nakamoto, K. Nakada, Y. Sato, K. Konishi, M. Hashizume, and S. Tamura, "Intraoperative magnetic tracker calibration using a magneto-optic hybrid tracker for 3-d ultrasound-based navigation in laparoscopic surgery," *Medical Imaging, IEEE Transactions on*, vol. 27, no. 2, pp. 255–270, 2008. (Cited on page 32.)

[62] P. A. Helm and T. S. Eckel, "Accuracy of registration methods in frameless stereotaxis," *Computer Aided Surgery*, vol. 3, no. 2, pp. 51–56, 1998. (Cited on pages 33 and 59.)

[63] R. R. Shamir, L. Joskowicz, S. Spektor, and Y. Shoshan, "Localization and registration accuracy in image guided neurosurgery: a clinical study," *International journal of computer assisted radiology and surgery*, vol. 4, no. 1, pp. 45–52, 2009. (Cited on page 33.)

[64] W. Elias, K. Fu, and R. Frysinger, "Cortical and subcortical brain shift during stereotactic procedures," *Journal of Neurosurgery*, 2007. (Cited on page 35.)

[65] D. Gering, A. Nabavi, R. Kikinis, N. Hata, L. O'Donnell, W. Grimson, F. Jolesz, P. Black, and W. Wells III, "An integrated visualization system for surgical planning and guidance using image fusion and an open mr," *Journal of Magnetic Resonance Imaging*, vol. 13, no. 6, pp. 967–975, 2001. (Cited on page 35.)

[66] A. Nabavi, P. McL Black, D. Gering, C. Westin, V. Mehta, R. Pergolizzi Jr, M. Ferrant, S. Warfield, N. Hata, R. Schwartz, *et al.*, "Serial intraoperative magnetic resonance imaging of brain shift," *Neurosurgery*, vol. 48, no. 4, p. 787, 2001. (Cited on page 35.)

[67] J. Mislow, A. Golby, and P. Black, "Origins of intraoperative mri.," *Magnetic resonance imaging clinics of North America*, vol. 18, no. 1, p. 1, 2010. (Cited on page 35.)

[68] R. C. Gonzalez, R. E. Woods, and S. L. Eddins, *Digital image processing using MATLAB*, vol. 2. Gatesmark Publishing Tennessee, 2009. (Cited on pages 37, 51, 52, 54 and 67.)

[69] L. G. Brown, "A survey of image registration techniques," *ACM computing surveys (CSUR)*, vol. 24, no. 4, pp. 325–376, 1992. (Cited on page 38.)

[70] J. L. Prince and J. M. Links, *Medical imaging signals and systems*. Pearson Prentice Hall Upper Saddle River, NJ, 2006. (Cited on pages 47 and 48.)

[71] M. Kachelrieß, "Micro-ct," in *Molecular Imaging I*, pp. 23–52, Springer, 2008. (Cited on pages 48 and 51.)

[72] C.-A. C. Inc., "http://www.carmcam.com/c-arms.html @ONLINE," June 2013. (Cited on page 49.)

[73] G. Wang, D. L. Snyder, J. O'Sullivan, and M. Vannier, "Iterative deblurring for ct metal artifact reduction," *Medical Imaging, IEEE Transactions on*, vol. 15, no. 5, pp. 657–664, 1996. (Cited on page 50.)

[74] R. A. Brooks and G. Di Chiro, "Beam hardening in x-ray reconstructive tomography," *Physics in medicine and biology*, vol. 21, no. 3, p. 390, 1976. (Cited on page 50.)

[75] Philips, "http://clinical.netforum.healthcare.philips.com/ @ONLINE," June 2013. (Cited on page 51.)

[76] Intuition, "http://www.inition.co.uk/3d-technologies/sensable-phantom-premium-10-15-and-30-models @ONLINE," June 2013. (Cited on page 58.)

[77] N. L. Dorward, O. Alberti, J. D. Palmer, N. D. Kitchen, and D. G. Thomas, "Accuracy of true frameless stereotaxy: in vivo measurement and laboratory phantom studies: technical note," *Journal of neurosurgery*, vol. 90, no. 1, pp. 160–168, 1999. (Cited on page 59.)

[78] D. V. Amin, K. Lozanne, P. V. Parry, J. A. Engh, K. Seelman, and A. Mintz, "Image-guided frameless stereotactic needle biopsy in awake patients without the use of rigid head fixation: Clinical article," *Journal of neurosurgery*, vol. 114, no. 5, pp. 1414–1420, 2011. (Cited on page 59.)

[79] R. Jain, R. Kasturi, and B. G. Schunck, *Machine vision*, vol. 5. McGraw-Hill New York, 1995. (Cited on pages 60 and 65.)

[80] J. M. Fitzpatrick, "Fiducial registration error and target registration error are uncorrelated," in *SPIE Medical Imaging*, pp. 726102–726102, International Society for Optics and Photonics, 2009. (Cited on pages 72, 74, 80 and 81.)

[81] J. B. West, J. M. Fitzpatrick, S. A. Toms, C. R. Maurer Jr, and R. J. Maciunas, "Fiducial point placement and the accuracy of point-based, rigid body registration," *Neurosurgery*, vol. 48, no. 4, pp. 810–817, 2001. (Cited on pages 72 and 73.)

[82] C. R. Maurer Jr, J. M. Fitzpatrick, M. Y. Wang, R. L. Galloway Jr, R. J. Maciunas, and G. S. Allen, "Registration of head volume images using implantable fiducial markers," *Medical Imaging, IEEE Transactions on*, vol. 16, no. 4, pp. 447–462, 1997. (Cited on page 72.)

[83] C. R. Maurer Jr, J. J. McCrory, and J. M. Fitzpatrick, "Estimation of accuracy in localizing externally attached markers in multimodal volume head images," in *Medical Imaging 1993*, pp. 43–54, International Society for Optics and Photonics, 1993. (Cited on page 72.)

[84] J. M. Fitzpatrick and J. B. West, "The distribution of target registration error in rigid-body point-based registration," *Medical Imaging, IEEE Transactions on*, vol. 20, no. 9, pp. 917–927, 2001. (Cited on page 72.)

[85] P. Kazanzides, G. Fichtinger, G. D. Hager, A. M. Okamura, L. L. Whitcomb, and R. H. Taylor, "Surgical and interventional robotics-core concepts, technology, and design [tutorial]," *Robotics & Automation Magazine, IEEE*, vol. 15, no. 2, pp. 122–130, 2008. (Cited on page 72.)

[86] J. M. Fitzpatrick, J. B. West, and C. R. Maurer Jr, "Predicting error in rigid-body point-based registration," *Medical Imaging, IEEE Transactions on*, vol. 17, no. 5, pp. 694–702, 1998. (Cited on pages 80 and 81.)

[87] R. D. Bucholz, H. W. Ho, and J. P. Rubin, "Variables affecting the accuracy of stereotactic localization using computerized tomography," *Journal of neurosurgery*, vol. 79, no. 5, pp. 667–673, 1993. (Cited on page 80.)